Peer-reviewed version available at *Materials* **2020**, *13*; doi:10.3390/ma13112586

Review

Magnetic nanomaterials as contrast agents for MRI

Sofia Caspani[1], Ricardo Magalhães[1], João P. Araújo[1] and Celia T. Sousa[1,*]

[1] IFIMUP and Dep. Física e Astronomia, Faculdade de Ciências Universidade do Porto, Rua do Campo Alegre 687, 4169-007 Porto, Portugal

* Correspondence: celiasousa@fc.up.pt

Abstract:

Magnetic Resonance Imaging (MRI) is a powerful, non-invasive and nondestructive tool, capable of providing three-dimensional (3D) images of living organisms. The use of magnetic contrast agents has allowed clinical researchers and analysts to enormously increase the sensitivity and specificity of MRI since these substances change the intrinsic properties of the tissues within a living body, increasing the information present in the images. The advances in nanotechnology and materials science as well as the research of new magnetic effects have been the driving forces that propel the use of magnetic nanostructures as promising alternatives to the commercial contrast agents used in MRI. This review discusses the principles associated with the use of contrast agents in MRI as well as the most recent reports focused on nanostructured contrast agents. The potential applications of gadolinium (Gd) and manganese Mn-based nanomaterials and iron oxide nanoparticles in this imaging technique are discussed as wel;, from their magnetic behavior to the mainly used materials and nanoarchitectures. Then, it is also addressed the recent efforts made to develop new types of contrast agents based on synthetic antiferromagnetic and high-aspect ratio nanostructures. Furthermore, the application of these materials in theragnosis, either as contrast agents and controlled drug release, contrast agents and thermal therapy or contrast agents and radiosensitizers, is also presented.

Keywords: nanomaterials, iron oxide nanoparticles, magnetic nanodiscs, synthetic antiferromagnetic nanostructures, nanowires, contrast agents, MRI, theragnosis.

Contents

1. Introduction

Magnetic Resonance Imaging (MRI) is a non-invasive powerful diagnostic technique used in medical science. This technique has several advantages, including extreme imaging flexibility, non-

ionizing radiation, patient harmlessness, high patient acceptance, high-resolution images with an excellent soft tissue contrast, provision of physiological parameters and acquisition of unique clinical information. As compared to other imaging modalities, the main advantage associated with this approach is its high spatial resolution, whereas its major drawback is the limited sensitivity of its probes [1]. Furthermore, over the last decades, numerous attempts have been made to improve the MRI sensitivity and facilitate biological as well as the functional information-rich imaging by the use of magnetic nanoparticles (NPs) and/or magnetic ions [2].

Gadolinium(III)-based contrast agents (GBCAs) are one of the most successful examples of MRI contrast agents. About 40% of MRI scans are performed with GBCAs and in the case of neuro MRI exams GBCAs are used in about 60% of them [3]. However, GBCAs have raised various toxicity concerns namely associated with a devastating and potentially fatal condition called nephrogenic systemic fibrosis. Also some fraction of the administrated GBCAs can remain in the organism for long periods, usually in form of Gd(III) [4]. Superparamagnetic iron oxide nanoparticles (SPIONs) have been developed and approved as viable alternatives to GBCAs. Such particles have various advantages, namely, biocompatibility, ability to be metabolized, relatively high saturation magnetic moments, and easy surface functionalization [5]. However, these contrast agents were not commercially successful [3]. This can possibly be attributed to the fact that the dimensions of such nanoparticles are restricted by the superparamagnetic regime, which limits the magnetic moment of each particle, and, through simulations, it is verified that the ideal particle size for MRI contrast agents surpasses such superparamagnetic threshold [6]. Among several nanomaterials that can be found in the literature with different shapes and compositions, magnetic nanostructures (MNS), in particularly nanodiscs and nanowires, are promising alternatives to SPIONs due to their larger magnetic moments that are not restricted by the superparamagnetic limit [7]. Also, MNS are a promising system for theragnostic since they can be used as contrast agents and at the same time generate a localized heating inside the body with the use of an external alternating current (AC) magnetic field or be used for controlled drug delivery, photodynamic therapy, and neutron capture therapy [8] and [9].

This review is focused on the recent advances in magnetic nanoparticles as contrast enhancing agents in MRI. Consequently, first we will discuss the principles of MRI regarding the use of T_1 and T_2 contrast agents, addressing, simultaneously, the contrast agents most commonly used in the clinical practice. Then, we explore the most recent efforts made to develop new types of contrast agents based on MNS: SPIONs, nanodiscs, synthetic antiferromagnets and high aspect ratio nanowires. Furthermore, the use of these nanostructures in both cancer diagnosis and therapeutics will also be discussed.

2. T_1 and T_2 contrast agents

MRI contrast agents enhance image quality by reducing the relaxation times of the nearby water protons and, consequently, changing the signal intensity of the water present in body tissues that contain the agent **[10]**. An MRI contrast agent normally shortens the rates of all the relaxation processes, however each substance predominantly influences one of them, therefore contrast agents that mainly shorten the relaxation time of the longitudinal component of the magnetization are called T_1 or positive contrast agents, while the T_2, or negative, contrast agents mainly reduce the relaxation time of the transverse component of the magnetization **[2]**. In general, two parameters are primarily used to evaluate the behavior of a contrast agent: longitudinal relaxivity (r_1) and relaxivity ratio, i.e. transversal relaxivity (r_2)/longitudinal relaxivity (r_1). Here, the value of r_1 indicates the signal enhancement potential of a contrast agent, while the r_2/r_1 ratio is an indicator of the suitability of a

contrast agent for positive (T_1) or negative (T_2) contrast. In general, T_1 contrast agents have a lower r_2/r_1 ratio (<5) while T_2 contrast agents have a larger r_2/r_1 ratio (>10) **[11]**.

T_1 contrast agents

The longitudinal relaxation reflects the energy loss from the spin system to its surroundings (lattice) and represents the realignment process of the longitudinal component of the magnetization with the external magnetic field. When a patient is submitted to a strong external magnetic field (B_0), the hydrogen nuclei, which are randomly oriented in the absence of the field, adopt one of two possible orientations: parallel or antiparallel to the external field. The energy difference between these two states is very small and originates a net magnetization vector (M_z) that does not produce any measurable signal due to its static equilibrium state. To obtain information from the spins, a radiofrequency (RF) pulse at the Larmor frequency, i.e. the frequency at which the nuclei freely precess about B_0, must be applied. Through this interaction it becomes possible to identify two relaxation processes, resulting from the application of a pulse that causes M_z to flip 90° from the positive z-axis to the transverse. After the RF transmitter is switched off, each individual magnetic moment will begin to precess about B_0 at their own Larmor frequency and the equilibrium state will be sought. This means that the transversal magnetization will decay over time, due to the dephasing of the magnetic moments, originating a decreasing signal, called free induction decay (FID), which oscillates at the Larmor frequency, and the longitudinal component of the magnetization will return to its initial maximum value along the direction of B_0 **[12]**. In this context, the T1 relaxation time provides a measure of how fast the net magnetization vector returns to its initial state parallel to B_0. This parameter is defined as the time required for Mz to recover to approximately 63% of its

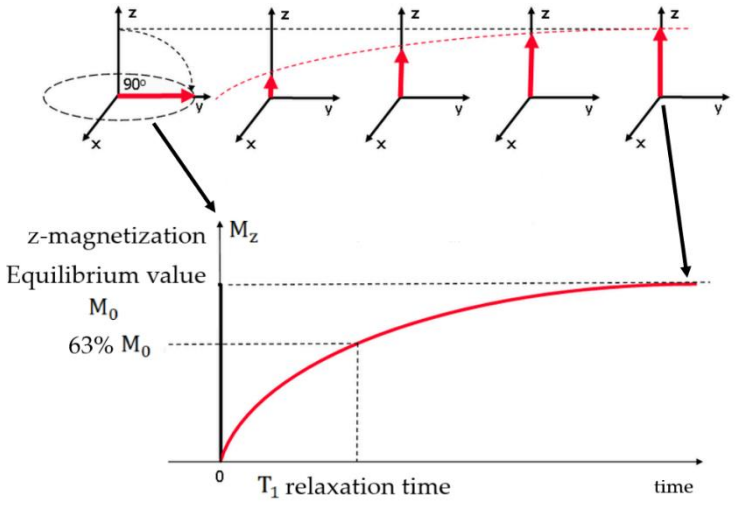

Figure 1: T1 relaxation process. Diagram showing the process of T1 relaxation after the application of a 90° RF pulse to a system at equilibrium. The z component of the net magnetization, M,z is reduced to zero, but then recovers gradually back to its equilibrium value if no further RF pulses are applied.

equilibrium value after the application of an RF pulse, as represented in Figure 1. Consequently, the MRI image can be improved by reducing the T_1 relaxation time, which originates a bright contrast in the acquired pictures. This can be achieved by using positive contrast agents, such as paramagnetic ions or materials.

Complexes of gadolinium (Gd(III)), manganese (Mn(II)) and iron (Fe (III)) are the most used paramagnetic T_1 contrast agents in MRI. Gd(III) has 7 unpaired electrons in the 4f subshell, whereas

Mn(II) and Fe(III) contains 5 unpaired electrons in the valence d orbitals. Nevertheless, all of them present high magnetic moments, large longitudinal electronic relaxation times (~10^{-8} s), and no magnetization in the absence of an external magnetic field **[13, 3, 10, 14]**. There are more transition metals and lanthanide metals with unpaired electrons, but for the metal to be effective as a relaxation agent the electron spin-relaxation time must match the Larmor frequency of the protons **[2]**. Additionally, the main problem associated with paramagnetic heavy metal ions in their native form is their toxicity **[15]**. Free Gd (Gd(III)), for instance, is very toxic and must be administered in its stable form to prevent the release of the metal ion *in vivo*. As a result, several types of GBCAs have been developed to satisfy these conditions **[13, 3]**. Of all the potential metal complexes that could be imagined, discrete Gd(III) chelates have been, so far, the most successful paramagnetic contrast agents so far and clearly dominate the contrast agents used in the clinic. Clinically used GBCAs can be categorised into three groups: extracellular fluid (ECF) agents, blood pool contrast agents (BPCAs) and organ-specific agents **[10]**. All GBCAs utilize an octadentate polyaminopolycarboxylato-based ligand and have a ninth coordination site available for water ligation. As an example, the commercially approved ECF GBCAs T1 contrast agents, for instance, are resumed in Table 1 **[3, 13]**

ECF agent (trade name)	ECF agent (chemical code)	ECF agent (generic name)	Approval date
Dotarem, Clariscan	Gd-DOTA	gadoterate meglumine	1989 Europe 2013 United States
ProHance	Gd-HPDO3A	gadoteridol	1992
Gadovist (Europe) Gadavist (United States)	Gd-DO3A-butrol	gadobutrol	1998 Europe 2011 United States
Magnevist	Gd-DTPA	gadopentetate dimeglumine	1988
Omniscan	Gd-DTPA-BMA	gadodiamide	1993
Optimark	Gd-DTPA-BMEA	gadoversetamide	1999
Multihance	Gd-BOPTA	gadobenate dimeglumine	2004

Table 1: commercially approved ECF GBCAs T1 contrast agents

To further reduce the toxicity of the free metal ions and have contrast agents that cross the blood brain barrier (BBB), the paramagnetic contrast agent research has focused on the development of nanostructured materials over the last few years **[14]**. Paramagnetic NPs present several advantages, such as the tuneability of size and shape, when compared to the contrast agents involving free metal ions, therefore many different approaches have been used to develop paramagnetic NPs for MRI. In general, the development of these NPs can be divided in two main classes, which are either the formation of nanoparticles with the paramagnetic ion incorporated into the nanostructured framework, such as $\boldsymbol{Gd_2O_3, Mn_3O_4, Dy_2O_3, MnO}$ **[16, 17, 18, 19, 20]**, or post-functionalisation of the NPs with lanthanide coordination complexes. This last approach has been developed together with

a number of supporting nanoparticle scaffolds (silica, gold, micelles and semiconducting quantum dots), which allow a subsequent doping with pentetic acid (DTPA), dodecane tetraacetic acid (DOTA), or derivates **[21, 22, 23, 24]**.

As the most successful inorganic metal developed in the context of nanomedicine so far, iron-based nanomedicine has been vastly approved in the medical realm, and recent efforts have been focused on the development of T_1 iron-based MRI **[25]**. Iron oxide NPs have been explored for decades due to their magnetic properties, biocompatibility and targeting potential. In contrast to the Gd-based contrast agents, iron oxide NPs are typically negative, i.e. T_2, contrast agents (e.g. superparamagnetic iron oxide NPs). These types of contrast agents are associated with low resolution and background interference, caused by body fluids and voids. Therefore, to overcome this problem, several studies have been carried out, leading to the development of ultrasmall iron oxide (USIO) NPs **[26, 27, 28, 29, 30, 5, 25, 31, 32]** and magnetic nanowires (NWs) **[28, 33, 34, 35, 36]**. The T_1 enhancement of USIO-NPs and NWs has been attributed to several possible factors, such as increased surface area, suppressed magnetization and surface effects on magnetization. Additionally, when the size of the nanoparticles is too small, their magnetization can be easily flipped by thermal energy. Under this condition, their behaviour is paramagnetic **[37, 38, 39, 40]**.

Besides the structures mentioned above, other types of structures have been accessed, such as stealth rare earth oxide nanodiscs **[41]**, linear arrays of magnetite nanoparticles **[42]** and antiferromagnetic compounds **[43, 18, 44]**.

T_2 contrast agents

The transverse relaxation depends on the spins precession frequency around B_0 and is defined by the T_2 relaxation time. This parameter represents the time interval during which the transverse magnetization decreases to approximately 37% of its initial value, as presented in Figure 2. Initially, after the excitation by the RF pulse, the spins precess completely in phase. But, as time passes, the observed signal starts to decrease, since the spins begin to dephase, due to small differences in the

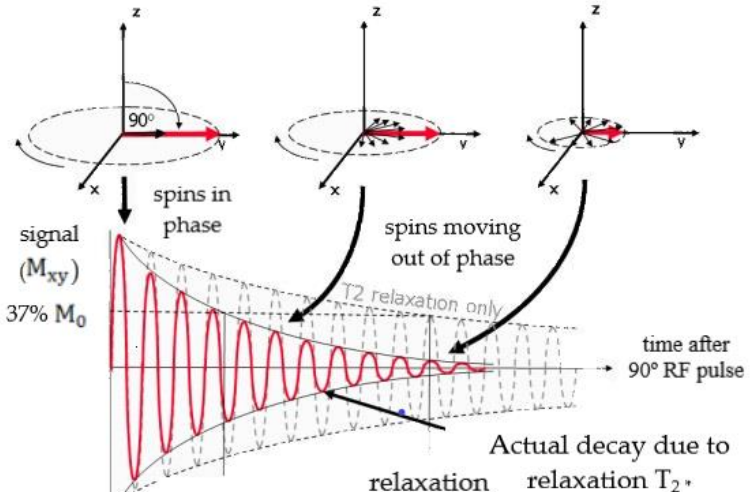

Figure 2: Transverse (T2 and T2*) relaxation processes. A diagram showing the process of transverse relaxation after the application of a 90° RF pulse to a system at equilibrium. Initially, the transverse magnetization (red arrow) has a maximum amplitude as the population of magnetic moments rotates in phase towards the xy plane. Then, the RF pulse is turned off and, subsequently, the amplitude of the net transverse magnetization (and therefore the detected signal) decays. The resultant decaying signal is known as the Free Induction Decay (FID).

Larmor frequency induced by the spin-spin interactions and the local magnetic environment of each proton, causing the T_2 relaxation, figure 2 **[45]**. However, in that same figure it is possible to verify that the real signal decays faster than the prediction based on the T_2 relaxation time. In fact, it is observed a faster exponential decrease as a function of a T_2^* time constant, which takes into account not only the intrinsic effects associated with T_2, but also the dephasing resulting from extrinsic magnetic inhomogeneities, such as defects within the main static magnetic field, B_0, or susceptibility differences between adjacent tissues. **[46]**

In this context, superparamagnetic iron oxides nanoparticles (SPIONs) have been developed as a viable alternative to the Gd(III)-complexes, and are widely studied by several authors **[47, 48, 10, 3, 39, 49, 50, 51, 52, 53]**. These nanostructures have various advantages, such as biocompatibility, ability to be metabolized, relatively high saturation magnetic moments and ease of surface functionalization **[54]**. Recently, it was also demonstrated that several types of nanoparticles were able to cross the BBB, increasing the possibility of early diagnosis of several diseases in the brain **[55]**.

Nevertheless, the dimension of such nanoparticles is restricted by the superparamagnetic limit, which implies a maximum diameter of per particle in order to maintain zero remanence, which is a fundamental property since it prevents the particles' aggregation in the absence of a magnetic field. For this reason, the magnetic moment of each particle is limited and, the ideal particle size for $\boldsymbol{T_2}$ MRI contrasts agents (20 nm **[6]**) usually surpasses the superparamagnetic limit **[56]**. Consequentially, to overcome these limitations, several authors have studied various alternatives namely high aspect-ratio ferromagnetic NPs **[36, 57]** and synthetic antiferromagnetic (SAF) nanostructures **[58]**.

3. Magnetic properties

The unique properties of NPs, , derive from the fact that these nanoscale magnets have high surface-to-volume ratios **[59, 60, 61]**. It has been demonstrated, in several studies, that saturation magnetization increases linearly with size until it reaches the bulk value. While the correlation between magnetization (M) and shape is not as direct, the effect of geometry on magnetic properties continues to be evaluated for biomedical applications. Based on the response of the intrinsic NP magnetic dipole and the net magnetization in the presence and absence of an applied magnetic field, NPs are typically classified as being either diamagnetic, paramagnetic, ferromagnetic, ferrimagnetic and antiferromagnetic **[59, 60]**.

Paramagnetic contrast agents

Paramagnetic contrast agents involve metal ions that have unpaired electrons, since materials whose atomic magnetic moments are uncoupled display paramagnetism **[14, 37, 10, 59, 60]**. The unpaired free electrons produce magnetic dipoles randomly aligned at equilibrium state, presenting an average magnetic moment equal to zero. Thus, paramagnetic materials have moments with no long-range order, as dipoles are aligned only upon the application of an external magnetic field, and they possess a small positive magnetic susceptibility **[59]**. Regarding their MRI application, paramagnetic nanomaterilas present several advantages over traditional coordination complexes, for instance their composition, size and shape are readily tuneable. The magnetic characteristics are improved by geometric local density effects rendering markedly higher T_1 and/or T_2 relaxometric values than the corresponding coordination complexes. In addition, pharmacokinetics enables a longer blood circulation time **[14]**.

In addition, it has been stated that paramagnetic properties can also arise from dimensional confinement. In the regime of a single magnetic domain (i.e. superparamagnetism), when the size of the particle is below a critical value, typically 5 nm **[26, 27, 28, 29, 30, 5, 25, 31, 32]**, the magnetization

can be easily flipped by the thermal energy. This leads to a T_1 improvement that can be attributed to various aspects, such as the suppression of the magnetization, , the increased surface iron center exposure, surface effects and water diffusion **[37]**.

Superparamagnetic nanoparticles

Superparamagnetism in SPIONs originates from the paramagnetic iron centers and is characterized by the presence of a large magnetic moment when applying an external magnetic field. **[47]**. In this case, all the magnetic moment in a particle compose a single domain, free to fluctuate in response to the thermal energy, while the individual atomic moments maintain their ordered state relative to each other. **[62]** This happens when the sample volume is reduced below a critical value, in which it costs more energy to create a domain wall than to support the external magnetostatic energy (stray field) of the single domain state. The magnetic anisotropy energy per particle, which is responsible for holding the magnetic moments along a certain direction, can be expressed as follows:

$$\mathbf{E(\theta) = K_{eff} V sen^2(\theta)}$$

where V is the particle volume, $\mathbf{K_{eff}}$ the anisotropy constant and θ is the angle between the magnetization and the easy axis. The energy barrier $\mathbf{K_{eff}}V$ separates the two energetically equivalent easy directions of magnetization. With decreasing particle size, it is reached a point where the thermal energy, $\mathbf{k_B}T$, exceeds the energy barrier $\mathbf{K_{eff}}V$ and the magnetization is easily flipped. As a result, for $\mathbf{K_{eff}}V < \mathbf{k_B}T$, the system behaves like a paramagnet, where instead of atomic magnetic moments, there is now a giant (super) moment inside each particle. This system is named a superparamagnet **[56, 48, 37]**. Such system has no hysteresis and the data of different temperatures superimpose onto a universal curve of M versus H/T **[63]**.
The relaxation time of the moment τ, is given by the Néel-Brown expression reported below; where $\mathbf{k_B}$ is the Boltzmann' constant, and $\boldsymbol{\tau_0 \approx 10^{-9}}$s.

$$\boldsymbol{\tau = \tau_0 exp\left(\frac{K_{eff} V}{k_B T}\right)}$$

If the particle magnetic moment reverses at times shorter than the experimental time scales, the system is in a superparamagnetic state, if not, it is in the so-called blocked state **[56, 48, 37, 62, 64]**, as presented in Figure 3.

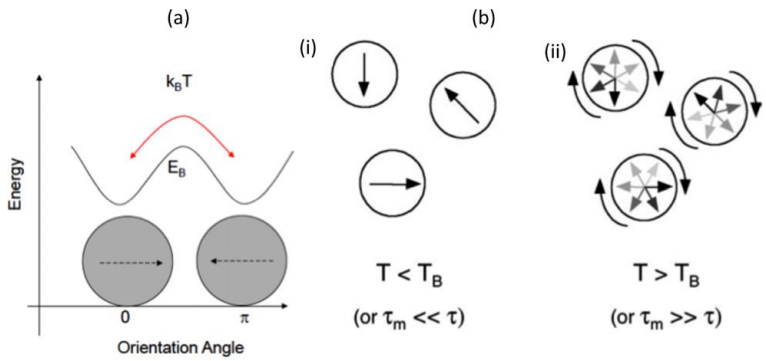

Figure 3: (a) Schematic of the energy barrier (EB) required for the magnetization of a nanoparticle to flip between the parallel and antiparallel orientations along the easy axis. (b) Illustration of particles in a (i) quasi-stable blocked and (ii) an unblocked freely rotating state

SAFs are a novel type of magnetic nanoparticles; their structure consists mainly in two ferromagnetic layers separated by a nonmagnetic one. The nomenclature of 'synthetic antiferromagnetic' refers to the anti-parallel alignment of the ferromagnetic layers, which then results in the near zero remanence at low fields **[65]**. The coupling between two ferromagnetic layers can be of two forms: magnetostatic or by interlayer exchange coupling. The first one strongly depends on the aspect ratio of the structure, while the second one depends on the material and the number of atomic layers **[66]**; Moreover, an oscillatory dependence on the thickness of the spacer has been found **[67, 68]**. Furthermore, SAFs are nanostructures optimized to have negligible remanence, low susceptibility around zero field and a distinct, tuneable, switch to full magnetization, which allows high saturation magnetization values at low applied fields **[65, 58, 69]**.

High aspect ratio nanowires

The unusual properties of nanowires (NWs) arises from their high-density of electronic states, enhanced surface scattering of electrons and photons, high surface to volume ratio and high aspect ratio. In comparison with others low-dimensional systems, NWs have two quantum-confined and one unconfined direction that allows to tune their magnetic properties, such as the orientation of the magnetic easy axis, Curie temperature, coercivity, saturation field, saturation magnetization and remanence magnetization **[7]**. Moreover, in NWs with multiple segments along their length, an antiferromagnetic coupling can be induced by controlling the separation between the magnetic layers **[70]** Their magnetic properties can be modified by changing the diameter, chemical composition and thickness of the segmented layers. NWs often appear as alternatives to the spherical NPs, as this geometry translates into intrinsic anisotropy properties that cause them to interact differently. **[71, 72, 73, 74]**. Moreover, they are characterized by increased surface to volume ratio and higher magnetic moments, originated from a prevalent shape anisotropy, which make them attractive for several biomedical biomedical applications such as contrast agents in MRI **[36]**.

4. Iron Oxide Nanoparticles

NPs are spherical nanostructures with a size between 1 and 100 nanometers, being comparable to biomolecules **[75, 76]**. Furthermore, they present unique physical, as well as chemical, properties, which arise from the fact that a great proportion of their atoms is present on the nanoarchitecture surface **[75, 77]**. Those distinct attributes, alongside the reduced size, have made these nanoformations a widely studied material in biomedicine, particularly as diagnostic, theranostic, or therapeutic tools **[77, 78]**. Nevertheless, only a few elements can be used for such applications due to toxicity problems **[76, 79]**. Within this context, iron oxide NPs have demonstrated a great potential, especially as MRI contrast agents, since they possess low toxicity, biodegradability, chemical stability under physiological conditions, and a fast response when an external magnetic field is applied **[76, 49]**. Consequently, various authors have been studying the use of these nanostructures in the context of that medical imaging technique.

An example is the work from Hobson *et al.* **[80]**, where SPIONs have been investigated as T_2 contrast agents. Particularly, here the goal was to improve the contrast produced by those NPs in T_2-weighted MRI. Therefore, 5 nm spherical nanoarchitectures have been fabricated via high temperature thermal decomposition, coated with oleic acid, and then agglomerated inside a self-assembling polymer (chitosan amphiphile) through physical means without cross-linking, forming raspberry SPIONs (Figure 4). After the synthesis process, it has been verified that these nanostructures were colloidally stable within various biomedical liquids. Afterwards, the MR relaxivities of single, as well as clustered, NPs have been measured, having been noticed an increase on their spin-spin (r_2) to spin-lattice (r_1) relaxation ratio (r_2/r_1) from 3.0 to 79.1 when grouping occurred, originating, therefore, a better negative contrast. Furthermore, the aggregated nanoarchitectures have been intravenously

administered to mice, to analyze their biodistribution and perform *in vivo* MRI studies. As a result, it has been observed that only the liver and the spleen accumulated the nanostructures, moreover these exhibited a blood half-life of 28.3 min. Additionally, the MRI tests have demonstrated an effective contrast, associated with these rasperry SPIONs, in the two organs where they were accumulated, providing clear images of the liver vasculature, including the portal vein, since they were localized in the extravascular space of that organ (Figure 5).

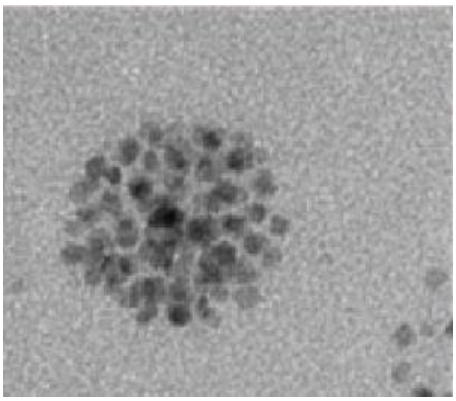

Figure 4: Transmission electron microscopy (TEM) image depicting a raspberry SPION, with a uranyl acetate (1%) staining *[80]*.

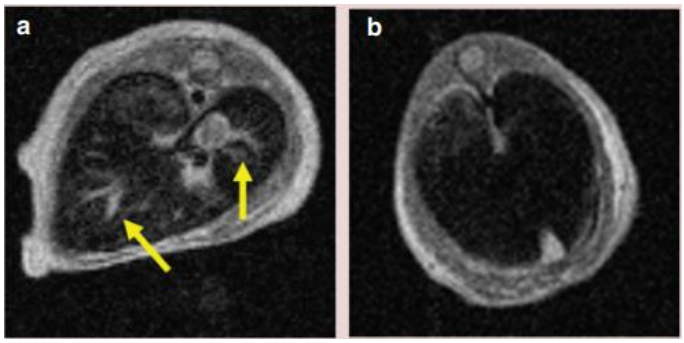

Figure 5: T_2-weighted axial MRI pictures illustrating a mice liver cross section 1 h after employing (a) raspberry SPIONs; (b) the commercially available contrast agent Ferucarbotran® *[80]*.

Another approach has been considered by Basly *et al.* **[81]**. Here, the authors have covalently bonded hydrophilic pegylated dendrons to SPIONs, using a phosphonate anchor (Figure 6). The dendritic molecules have been selected because they were discrete and monodisperse entities, not only exhibiting adjustable characteristics, but also permitting distinct as well as reproducible polyfunctionalizations at their periphery. On the other hand, the phosphonate coupling agent has been chosen since it provided a strong binding, stabilized suspensions within water possessing a physiological pH, and conserved the magnetic properties of the nanostructures. Then, the relaxivities associated with these nanoarchitectures have been analyzed considering a 1.5 T magnetic field. As a result, the authors obtained a r_2/r_1 ratio equal to 44.8, having measured relaxivity values 1.5 times higher than those exhibited by commercially available polymer-decorated NPs. Additionally, *in vitro* relaxivity measurements, under 7 T, confirmed a significant negative contrast.

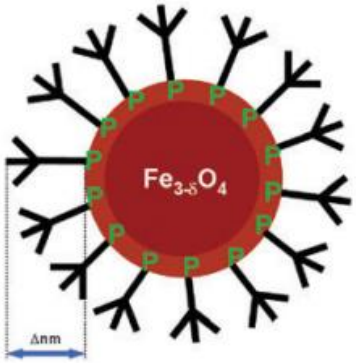

Figure 6: Illustration representing a hydrophilic pegylated dendrons covalently bonded to an iron oxide nanoparticle, via a phosphonate anchor *[81]*.

Xie *et al.* **[82]** have performed a different study, where a MRI contrast agent for identifying brain *gliomas in vivo*, i.e. lactoferrin-conjugated SPIONs (LfSPIONs), has been developed. After synthesizing such NPs, the authors have examined their physical, chemical, and magnetic properties, as well as their interaction with glioma cells. As a result, it has been verified a hydrodynamic diameter equal to ~ 75 nm, a 51 emu/g Fe saturation magnetization, plus a T_2 relaxivity of 75.6 $mM^{-1}s^{-1}$, for these spherical nanostructures. Additionally, an *in vitro* study, considering a rat glioma cell line (C6), revealed that the Lf-SPIONs originated MR images possessing a better T_2 contrast than the one produced by SPIONs. Furthermore, an *in vivo* investigation has been performed using rat models together with the developed NPs. It has been noticed a considerably improved contrast, between the tumor and the neighboring normal tissues, on T_2-weighted brain glioma MR images, until 48 h after the Lf-SPIONs administration (Figure 7). Following such time period, a histochemical analysis hasallowed the observation of those nanostructures around the vascular region of the lesion tissue slices. Moreover, real-time polymerase chain reaction (RT-PCR) plus Western Blot have been employed in the brain tumor tissues. These techniques have allowed the authors to confirm a larger expression level associated with Lf receptors, when compared against normal tissues from the same organ. Consequently, these results have indicated that Lf-SPIONs are suitable T_2 MRI contrast agents for brain glioma, presenting high selectivity and sensitivity.

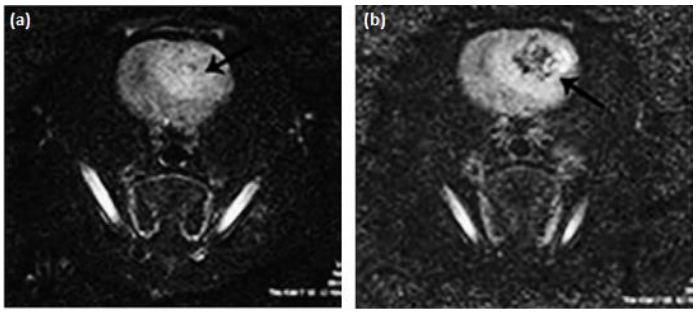

Figure 7 - *In vivo* T2-weighted MR images of rats' brain possessing C6 gliomas, acquired 48 h after the administration of SPIONs; Lf-SPIONs *[82]*.

In a different work, Gonzalez-Rodriguez *et al.* **[83]** have fabricated biomcompatible SPIONs conjugated with graphene oxide (GO-SPIONs). These spherical nanostructures have presented a mean size of 250 nm and have demonstrated the ability to be used towards magnetic targeted therapy, fluorescence imaging, cancer detection via optical pH-sensing, anticancer drug delivery, as well as MRI contrast agents. Cytotoxicity assays have revealed a reduced cell death resulting from the

nanoparticles internalization, at a 15 g/mL concentration. Furthermore, relaxivity measurements have indicated a r_2/r_1 ratio of ~ 10.7 for the GO-SPIONs, being considerably higher than the one exhibited by free SPIONs (~ 2.3). Consequently, this suggested that the graphene oxide conjugated SPIONs have had the potential to be employed as T_2 MRI contrast agents. Additionally, the authors have successfully distinguished cancer cells from healthy ones *in vitro* through the ratios of emission intensity associated with NPs, since they presented fluorescence in the visible range that depended on the medium pH (Figure 8). Concerning drug delivery, it has been achieved a successful fluorescence-tracked intracellular delivery of hydrophobic doxorubicin non-covalently conjugated with GO, by applying an external magnetic field. This have resulted in a 2.5-fold efficacy enhancement, when compared against the free drug at reduced concentrations, becoming possible to reduce the drug dose required for reaching an identical therapeutic effect.

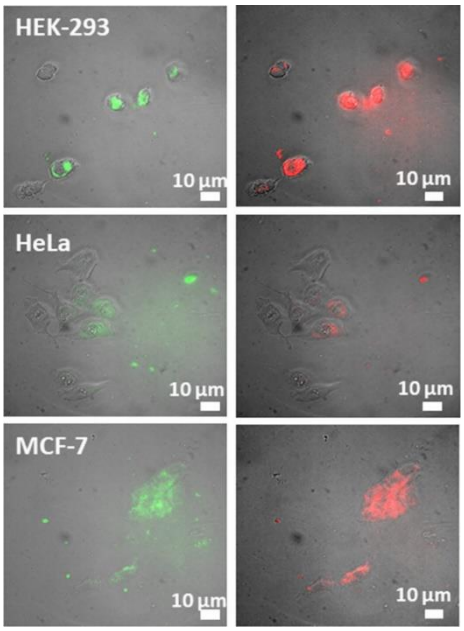

Figure 8 - Pictures representing the GO-SPIONs emission in green (550 nm) and red (635 nm) in healthy HEK-293 versus cancer HeLa and MCF-7 cells [83].

Also considering SPIONs, Sulek *et al.* **[84]** have fabricated a contrast agent by a non-covalent functionalization of those nanoparticles with peptide amphiphile molecules, which provided water solubility and improved their biocompatibility (Figure 9). Then, after production, the nanocomplexes relaxivity has been assessed under a 3.0 T magnetic field, having been observed a r_2/r_1 ratio as high as 111.55, being a much larger value than that of commercially available SPIONs. Furthermore, *in vitro* incubation experiments using fibroblasts (NIH 3T3) have revealed that these functionalized NPs were, in fact, highly biocompatible. Moreover, it has been observed that such spherical nanostructures were located on the cell membrane or matrix. Additionally, the hydrophilic peptide sequence located at the SPIONs surface, which has supplied stability as well as bioactivity within aqueous conditions, could be changed so as to target them towards specific tissues.

A different T_2 contrast agent, i.e. multifunctional polymeric-coated multicore NPs (bioferrofluids), has been investigated by Ali *et al.* **[85]** .These spherical nanostructures have consisted in various maghemite NPs involved with a hydrophilic polymer (polyethylene glycol, PEG, acrylate). Furthermore, their uptake and toxicity in the liver of mice has been assessed through MRI together with histological techniques. Then, the obtained outcomes have been compared against those acquired when employing commercially available Endorem magnetic fluids, under identical

experimental circumstances. As a result, it has beenverified that the r_2/r_1 ratio for the bioferrofluids synthesized by the authors was equal to 184, while for Endorem such parameter exhibited a value of 54.02. Additionally, these NPs not only exhibited a smaller blood circulation period, but also have demonstrated to be efficient reticuloendothelial system agents, since they remained in the liver tissue. Moreover, it has been observed that those bioferrofluids stayed in such organ for a longer time interval than Endorem. Nevertheless, no perceptible histological lesions in the examined liver were caused by the two contrast agents analyzed, over a time interval of 60 days after-administration.

Another type of contrast agent has been analyzed by Zhang *et al.* **[86]**. This nanomaterial has consisted in SPIONs coated with polyethylenimine (PEI), which were obtained through photochemistry, and whose surface was modified by poly(ethylene glycol) methyl ether (MPEG), MPEG-PEI-SPIONs (Figure 9). Then, the physical properties, stability, as well as MRI feasibility of these NPs have been assessed. It has been verified that they possessed a hydrodynamic size equal to 34 nm. Furthermore, their coating has been checked through a Fourier transform infrared spectrometer, having been determined a 31% and 12% proportion of PEI and MPEG, respectively, in the MPEG-PEI-SPIONs. Additionally, magnetic measurements showed a superparamagnetic behavior, as well as 46 emu/g saturation magnetization, for these nanoarchitectures. Furthermore, a stability test has indicated that MPEG-PEI considerably enhanced the spherical nanostructures stability. Moreover, relaxation measurements have demonstrated similar r_2 values for PEI-SPIONs and MPEG-PEI-SPIONs. Additionally, T_2-weighted MR images using MPEG-PEI-SPIONs have revealed a considerable improvement of the MR signal, as the concentration of those NPs in water got higher. Consequently, this indicated that these spherical nanostructures have been able to produce large magnetic field gradients near their surface.

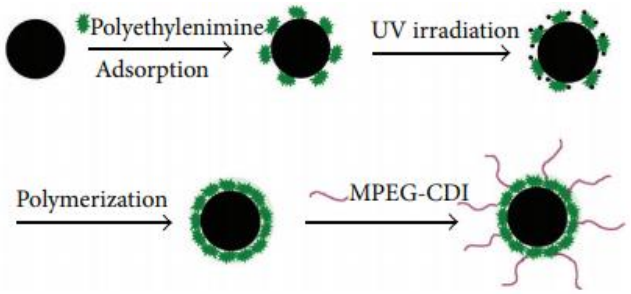

Figure 9: Schematic representation of the MPEG-PEI-SPIONs fabrication process *[86]*.

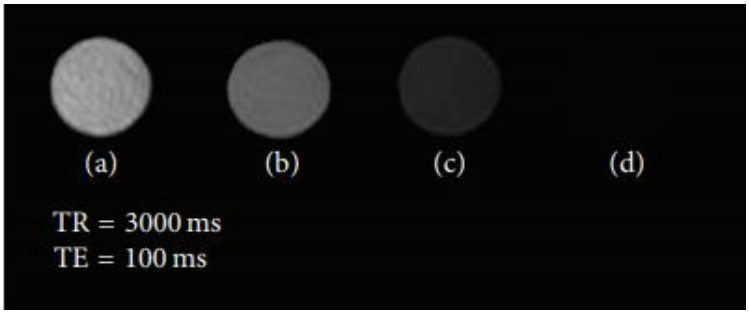

Figure 10: T2-weighted MR images of MPEG-PEI-SPIONs considering different concentrations, namely (a) 0.063; (b) 0.125; (c) 0.250; (d) as well as 0.500 mg/mL *[86]*.

Yue-Jian *et al.* **[87]** have addressed a novel contrast agent consisting in antifouling PEG-coated SPIONs. Here, monodisperse oleic acid-coated SPIONs have been synthesized via thermal decomposition of iron oleate. Then, the self-assembly occurring between those spherical

nanostructures and the PEG-lipid conjugates in water. It has been observed, through dynamic light scattering, that the PEG-coated SPIONs were stable within water for a pH from 3 unto 10 and at sodium chloride concentrations up until 0.3 M. Furthermore, their incubation with a cell culture medium possessing 10% fetal bovine serum, which simulated the *in vivo* plasma, has confirmed such stability, not having been noticed changes in the NPs dimensions after a 24 h time period. These results have pointed out an absence of protein adsorption upon their surface. Moreover, *in vitro* relaxation measurements have indicated a greater r_2 for these spherical nanoarchitectures than that of the commercially available contrast agent Feridex IV, suggesting, therefore, that a better contrast could be created by these PEG-coated SPIONs.

Several authors have also gained interest for the use of iron oxide NPs as T_1 contrast agents, since in the clinical practice the typically employed positive contrast agents are Gd complexes, which, as previously referred, pose health risks to the patients **[88, 10, 89, 5]**. Within this context, Wei *et al.* **[90]** have investigated zwitterion-coated SPIONs (ZES-SPIONs), possessing inorganic cores with a size of ~ 3 nm as well as an ultrathin hydrophilic shell (~ 1 nm). As a result, it has been verified that these NPs presented a r_2/r_1 ratio equal to 2.0, being a value lower than the one associated with other SPION-based positive contrast agents, nevertheless it was within a factor of 2 to that exhibited by Gd-based chelates. Additionally, *in vivo* MRI has been performed on mice injected with ZES-SPIONs, to assess their preclinical potential as T_1 contrast agents for MRI and MR angiography. These tests have revealed a contrast power, associated with those NPs, that was sufficiently high for their use in the considered applications. Moreover, it has been observed an efficient renal clearance of the ZES-SPIONs and, by measuring once again their r_2/r_1 ratio after excretion, the authors have verified that the MR contrast power of those NPs was kept largely unmodified under physiological conditions.

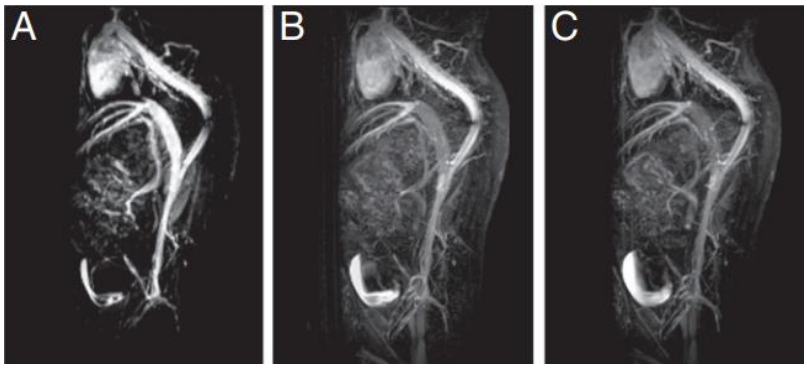

Figure 11: T1-weighted MR angiography, at 7 T, of a mouse (a) 4 min; (b) 12 min; and (c) 20 min, after the injection of ZES-SPIONs *[90]*.

Yin *et al.* **[91]** have achieved a T_1 contrast in MRI by employing SPIONs, with diameters between 11 and 22 nm, in a ultra-low feld (ULF) MRI system, which applied a ~ 0.13 mT magnetic field, at room temperature. This approach has allowed improving the positive contrast created by such NPs, because under these conditions their relaxation times were similar to the proton Larmor precession period, originating a great increase of the r_1 value. Additionally, their r_2 was lowered, since the magnetic moments, present in the SPIONs, were not saturated at this field magnitude. As a result, a r_1 as high as 615 $mM^{-1}s^{-1}$ has been obtained for $Zn_{0.3}Fe_{2.7}O_4$ NPs, coated with silicon dioxide, and possessing a size of 18 nm, being a value 100 times larger than that of typical commercial Gd-based positive contrast agents under large magnetic fields, i.e. 1.5 and 3.0 T. Furthermore, the authors have verified a linear dependence of r_1 on the imaginary part of the magnetic AC mass susceptibility, at 5.56 kHz, i.e. the proton resonance frequency, for all the studied cases. This result has been justified by the NPs magnetic fluctuations, associated with Brownian motion or Néel relaxation. As a

Peer-reviewed version available at *Materials* **2020**, *13*; doi:10.3390/ma13112586

conclusion, various benefits have been observed for this approach, namely adjustable magnetic susceptibility in SPIONs, improved signal, shorter imaging times, as well as the use of biocompatible substances.

Another work by Corr et al. **[42]** have addressed suspensions of linear chains of magnetite NPs, produced by the cross-linking of surrounding particles with polyelectrolyte molecules and the application of an external magnetic field, for biomedical application. Through the application of an external magnetic field, it has been verified that these nanostructures have rearranged into parallel arrays Then, their relaxivity has been measured using field-cycling NMR at 37 °C, having been observed a considerable reduction in the relaxation times for all the considered fields. The authors also acquired MR images of live rats, injected with these nanoarchitectures, so as to assess their effect on the rodents' brain. The obtained results have proved that these nanostructures had a good biocompatibility and could be employed as contrast agents for *in vivo* MRI, having darkened the brain regions in a T_1-weighted MR image, as shown in Figure 12.

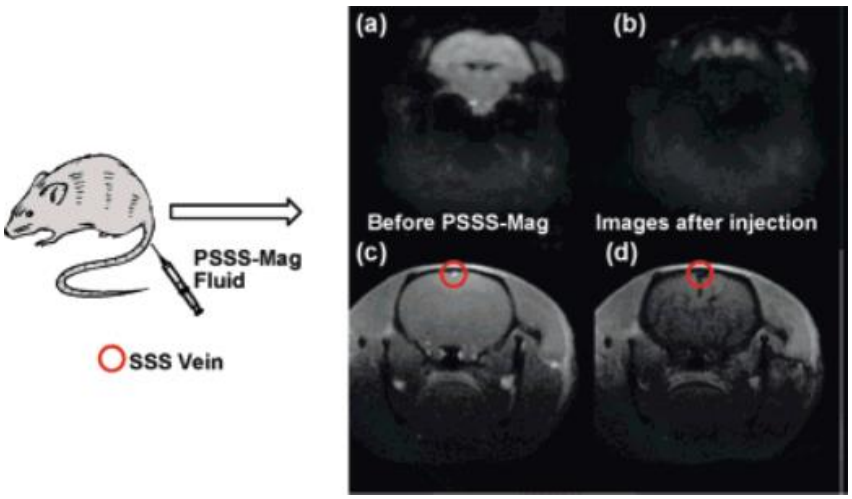

Figure 12: Echo planar image (EPI) of a mouse brain (a) before and (b) as PSSS-Mag1(Fe/Polysodium-4-styrene sulfonate ratio 1:2) passes through the organ; Fast Low Angle Shot (FLASH) image of mouse brain (c) before and (d) as PSSS-Mag1 passes through the organ *[42]* .

Yeast derived β-glucan particles (GPs) are a class of microcarriers, under development, with the capability to target cells of the immune system, allowing, for example, the delivery of drugs or imaging agents to those biological entities. However, encapsulation those compounds in the porous GPs is challenging. In this context, Patel *et al.* **[43]** have produced high spin Fe(III) macrocyclic complexes that function as effective *in vivo* T1 MRI contrast agents. As a result, it has been shown that the unique coordination chemistry of the Fe(III)-based macrocyclic T_1 MRI contrast agents permitted their facile encapsulation in GPs. Remarkably, the GPs labelled with the simple Fe(III) complexes were stable under physiologic conditions. Additionally, in contrast to the free Fe(III) coordination complex, the labelled Fe(III)-GPs have lowered the T_1 relaxivity and acted as a silenced form of the contrast agent.

4. Gd and Mn-based nanomaterials

A broad range of approaches have been applied to the incorporation of Gd chelates into nanoparticles **[14]**. Of them, gadolinium-doped silica nanoparticles have been extensively reported. In this context, Rieter et al. **[92]** have produced stables nanoparticles with r_1 values greater than those of conventional Gd chelates by the utilization of a luminescent core $\mathbf{[Ru(bpy)_3]Cl_3}$ with a silylated Gd complex

coating. Another work has demonstrated that the location of the Gd chelate within mesoporous silica nanoparticles (MSNs) greatly influences its relaxometric properties. The highest relaxivities have been specifically reported to occur when synthesis occurs by a long delay co-condensation process, leading to a r_1 value of 33.6 ± 1.3 $\mathbf{mM^{-1}s^{-1}}$, which is higher than any previously reported Gd-DOTA silica NPs and 20 times larger than free Gd-DOTA **[93]**. Then, these particles were biotinylated showing a large relaxivity that was kept after the external biomodification, but presenting reversibly gateable on subsequent protein recognition **[94]**. Graphene oxide (GO) has also been used as a scaffold to integrate Gd-DOTA moieties. A study by Zhang et al. **[95]** reported that GO has been first pegylated, functionalised with DOTA, and then metallated with Gd(III). These nanoparticles have presented a large r_1 value of 14.2 $\mathbf{mM^{-1}s^{-1}}$measured at 11.7 T. Some other strategies to incorporate Gd in several types of nanoparticles have also been reported, namely by grafting Gd(III) in detonation nanodiamond (DND) **[96]** and melanin-dots (M-dots) loaded with Gd (II) **[97]**

Gadolinium oxides are the most utilised alternatives to Gd chelates, where it has been found that decreasing particle diameter resulted in a progressive trend towards higher relaxivities. For instance, Park et al. **[17]** have shown that the highest relaxivities were obtained for NPs synthesised with an average diameter, *d*, of ~ 1–2.5 nm, as presented in Figure 13. As a result, high contrast in *in vivo* T_1 images of the brain tumour of a rat have been observed. The large r_1 has been discussed in terms of the big surface to volume ratio of the ultrasmall gadolinium oxide nanoparticles, coupled with the cooperative induction of surface Gd(III) ions for the longitudinal relaxation of a water proton. It should be noted, however, that ultrasmall $\boldsymbol{Gd_2O_3}$ NPs have been found to form deposits in the brain and, consequently, there is a compromise between limiting the toxicity of the particles and maximising imaging potency. Yin et al. **[98]** have produced silica nanoparticles with a $\boldsymbol{Gd_2O_3}$ nanoshell of varying thicknesses. By systematically changing the thickness of the silica shell, the variations in relaxivity values could be investigated and it was demonstrated that a thinner shell resulted in larger r_1 values. Furthermore, the core-shelled nanoparticles showed negligible nanotoxicity. The enhanced signals in *in vivo* tumour-targeted MRI indicated that ultrathin gadolinium oxide nanoshells may function as a potential candidate for advanced positive contrast agents in further clinical applications.

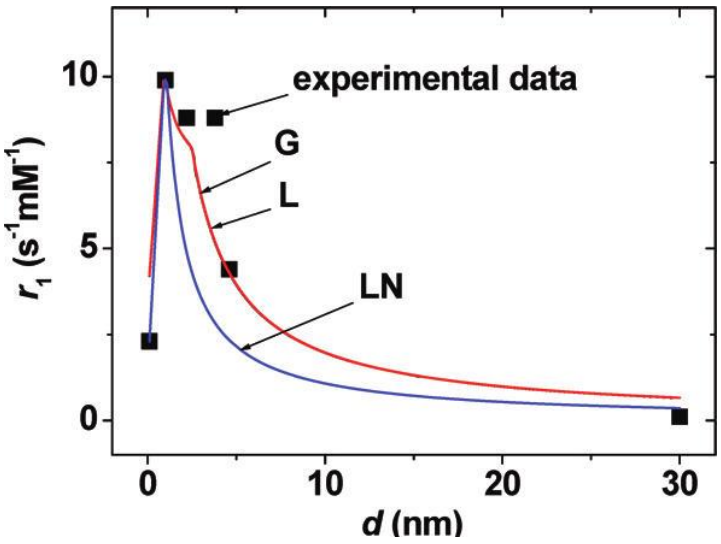

Figure 13: Reproductions of r_1. The functions are labeled as G (Gaussian), L (Lorentzian), and LN (log-normal) [17].

Dual T_1- and T_2-weighted MRI agents were also reported by Zeng *et al.*. Such authors fabricated biocompatible gadolinium hybrid iron oxide (GdIO) nanocomposites with hydrodynamic size between 120 and 150 nm. These nanocomposites exhibited both superparamagnetic and paramagnetic properties, with unsaturated magnetic moments of 33.5 emu g^{-1} at 5 T. The GdIO samples exhibited high contrast ability for both T1 and T2-weighted MR imaging, with r_1 value of 70.10 ± 3.65 mM^{-1} s^{-1} (based on Gd) and an r_2 value equal to 173.55 ± 6.48 mM^{-1} s^{-1} (based on Fe). *In vivo* studies showed that the GdIO nanocomposites were able to achieve the brain tissues and translocate into neurons **[99]**.

Bailey et al. **[41]** have reported the fabrication of $\boldsymbol{RE_2O_3}$-based nanodiscs, with diameters ranging from 10 to 14 nm; RE stands for Gd, dysprosium (Dy) or ytterbium (Yb) passivated with a biocompatible polymer (Poly(acrylicacid) grafted with short methoxy-terminated polyethylene oxides). Here, their suitability as MRI contrast agents has been analysed. The relaxation times of such nanostructures, measured at 37 °C (body temperature) in a magnetic field of 1.41 T, have been compared to the reported values for their spherical counterparts or small molecule chelates, based on the DTPA ligand. The authors have also performed an MR scan of a phantom for all the considered contrast agents, using $\boldsymbol{T_1}$ weighted sequences, having been found that $\boldsymbol{Gd_2O_3}$ nanodiscs were more suitable as contrast agents compared than the commercially available Gd-DTPA, due to their higher relaxivities **[100]** . This factor should increase the efficiency of *in vivo* targeted imaging schemes, since it becomes possible to get a high amount of proton relaxation without requiring multiple small molecules in contact with the imaging target. Besides this benefit, it has been verified that these $\boldsymbol{Gd_2O_3}$ nanodiscs were suitable as $\boldsymbol{T_1}$ contrast agents. Also, no significant cytotoxic effects have been observed for the polymer coated $\boldsymbol{Gd_2O_3}$and $\boldsymbol{Dy_2O_3}$ nanoarchitectures, on a cell line derived from a human cervical cancer (HeLa).

Singh et al. **[20]** also reported the suitability of polyethylene glycol (PEG) coated $\boldsymbol{Gd_2O_3}$ paramagnetic nanodiscs and PEG coated Gd doped iron oxide (GdIO) superparamagnetic cubic/spherical-shaped nanoparticles, with different dimensions, as MRI contrast agents. In this case, the relaxivities of the different nanoarchitectures have been measured with a 7 T MR scanner and it has been showed that smaller sized nanostructures (<5 nm) were the more effective $\boldsymbol{T_1}$ contrast agents, as presented in figure 14.

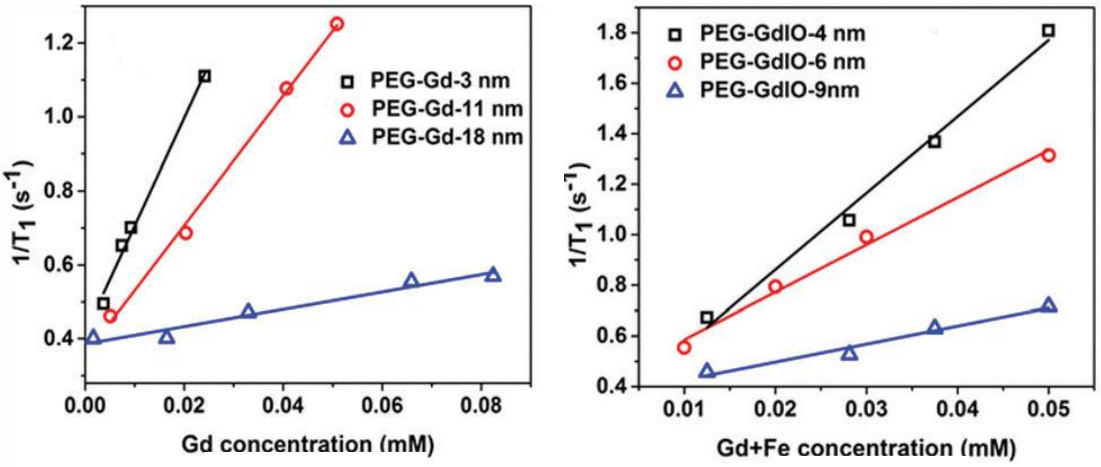

Figure 14: T1 relaxation rate as a function of concentration measured for (a) Gd_2O_3 nanodiscs of different diameters and (b) GdIO NPs of spherical (9 nm and 6 nm) and cubic (4 nm) shapes [20].

Besides Gd-based nanoparticles, Mn has also been extensively researched as a possible T_1 contrast agent with reduced toxicity (compared to that of Gadolinium), but it possesses low native r_1 relaxivities. Nevertheless, it has shown promising results as dual modal imaging agent, as presented in Figure 5 [14]. Much effort has been invested in increasing and biocompatibility and r_1 by using derived nanoparticulate systems. For instance, PEG-functionalised Mn_3O_4 nanoparticles have been encapsulated in a mesoporous, biocompatible carbon framework. Then, it was demonstrated that the agent displayed significant contrast enhancement in T1-weighted images. The carbon encapsulation and surface modification rendered biocompatibility and water solubility to the nanosystem. Furthermore, the porous network ensured water accessibility for the nanoparticles, making them helpful in interpretation of MRI scans [101].

Neves *et al.* **[44]** have addressed Mn oxide (MnO) NPs (average size of ~ 20 nm) coated with carboxymethyl-dextran. Despite not having performed an *in vivo* study, the authors have considered such nanostructures adequate as T_1 contrast agents, due to their significant longitudinal relaxivity, measured on a clinical 3.0 T MRI scanner. Moreover, it has been observed that such NPs presented no *in vitro* cytotoxicity for healthy cells at concentrations lower than 25 μg/ml, however for HeLa cells a notable toxicity has been observed, even at low concentrations of NPs (5 μg/ml).

Manganese ferrite nanoparticles (Fe3O4@MnIO) have also exhibited remarkably higher longitudinal relaxivity than their counterpart iron oxide NPs [102]. Here, the authors found a r_1 value of 33.8 $mM^{-1}s^{-1}$ for Fe3O4@MnIO and a r_2 equal to 306.3 $mM^{-1}s^{-1}$. The increased T_1 relaxivity was attributed to the extended electronic relaxation time and the increased number of unpaired electrons due to the Fe substitution by Mn ions. Additionally, *in vivo* results indicated that these nanoparticles could achieve *in vivo* contrast imaging with acceptable biocompatibility, with the dosage of 1 mg/kg, however the systemic toxicity evaluation was unclear.

5. Synthetic antiferromagnetic nanostructures

More recently, antiferromagnetic nanoarchitectures have also been investigated as potential T_1 contrast agents by different authors. Namely, Na *et al.* **[18]** fabricated antiferromagnetic MnO nanoparticles of sizes between 7 and 25 nm, coated with a PEG-phospholipid shell. The relaxivity of such particles has been measured in a 3.0 T human clinical scanner and their *in vivo* performance as MRI contrast agents has been analyzed in a mouse. The obtained results have indicated that these NPs were suitable as T1 contrast agents, having demonstrated no significant toxicity, for a MnO concentration lower than 0.82 mM, in eight human cell lines originating from different tissues. Furthermore, by conjugating them with a tumour-specific antibody, it has been possible to selectively improve the contrast of breast cancer cells located in a mouse's metastatic brain tumour, which has been intravenously injected with the functionalized nanoparticles through T_1-weighted MRI.

Liuet *et al.* **[103]** have also fabricated spherical nanostructures exhibiting antiferromagnetic properties towards the same application. These nanoarchitectures were glutathione-functionalized iron-oxide nanoparticles, having been produced at room temperature and in aqueous-phase, by a facile, highly efficient, as well as eco-friendly, one-step reduction process, using tetrakis(hydroxymethyl)phosphonium chloride as the reducing agent. After the synthesization

procedure, the nanostructures characterization has revealed a diameter of 3.72 ± 0.12 nm, an r_2 equal to 8.28 $mM^{-1}s^{-1}$, a 2.28 r_2/r_1 ratio, a reduced magnetization, plus an adequate water dispersion. Additionally, through their incubation with HeLa cells, it has been observed that they were biocompatible and improved the acquired MR signal intensity, in T_1-weighted sequences, as the iron content inside the considered biological entities increased. Moreover, the fabricated nanoparticles havealso been injected into mice as well as rat models, so as to not only study their *in vivo* circulation and metabolic path, but also to analyze the contrast created by them in MR images, under those conditions. As a result, it has been observed that the nanostructures escaped the hepatic reticuloendothelial system and, subsequently, were expelled from the body via the urinary system, enabling, therefore, the realization of a renal function assessment. This course led to a long circulation period in the vasculature, allowing a strong improvement, in T_1-weighted MRI, of the vascular resolution at the internal carotid artery and superior sagittal sinus, which are locations where the thrombus identification is essential for diagnosing a stroke (figure 15). Additionally, various T_1- as well as T_2-weighted MR images of a rat's kidney injected with the produced nanostructures, allowed a detailed visualization of the cortical-medullary anatomy and renal physiological functions.

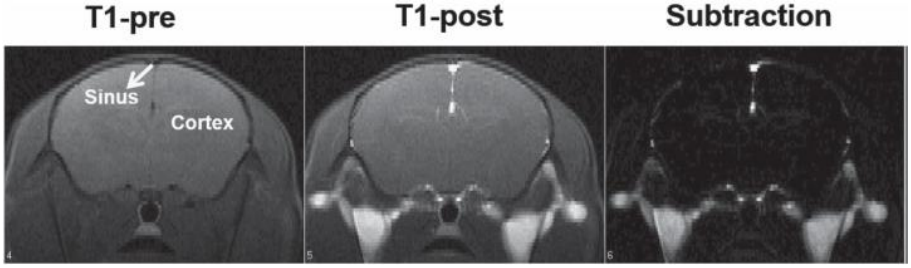

Figure 15: T_1 –weighted MR images of a mice´s brain, before (T_1-pre) and after (T_1-post) the injection of the glutathione-functionalized iron-oxide nanoparticles *[103]*.

In a different work, Peng *et al.* **[43]** have investigated another T1 contrast agent type, known as antiferromagnetic-iron oxide-hydroxide nanocolloids, which possessed a diameter of 2-3 nm. Such nanostructures have been prepared in the mesopores of worm-like mesoporous silica. Then, the relaxation times have been measured at 40 °C using a 0.47 T Minispec spectrometer. As a result, it has been verified that these nanoparticles not only had the lowest r_2/r_1 ratio reported, until 2013, for iron-based colloidal T_1 contrast agents, but also possessed a considerably large longitudinal relaxivity. Additionally, the acquired MR images have shown that such nanocolloids were a superior T_1 contrast agent, in both *in vitro* (HeLa cells) and *in vivo* (rat and mouse) MRI, when compared to ultrasmall iron oxide nanoparticles. Furthermore, these nanocolloids also demonstrated a high level of biocompatibility and biodegradability.

In addition to the previously mentioned nanoarchitectures, (SAF nanostructures have also been studied as potential contrast agents for MRI. For example, Roosbroeck *et al.* **[58]** have fabricated phospholipid-coated, disc-shaped, and multilayered [Au(10 nm)/Ni80Fe(5 nm)20/Au(2.5 nm)/Ni80Fe(5 nm)20/Au(10 nm)] SAF nanoarchitectures, with diameters ranging from 89.8 nm to 523.2 nm, using a colloidal lithography technique. The magnetic characterization of these nanodiscs has indicated a very low remanence value, which is necessary to prevent particle agglomeration, as well as a high magnetization, making them adequate for biomedical applications. Then, these nanostructures have been evaluated as T_2 contrast agents, as indicated in Figure 16, having shown improved relaxivities, at 24.85 °C in a 9.4 T magnetic field, when compared to SPIONs, especially the smallest particles with a diameter of 90 nm. The authors have also carried out an *in vitro* MRI study, using an ovarian cancer cell line (SKOV3), confirming the increased T_2 relaxation for cells marked with such nanostructures.

Preprints (www.preprints.org) | NOT PEER-REVIEWED | Posted: 28 April 2020 doi:10.20944/preprints202004.0490.v1

Peer-reviewed version available at Materials 2020, 13; doi:10.3390/ma13112586

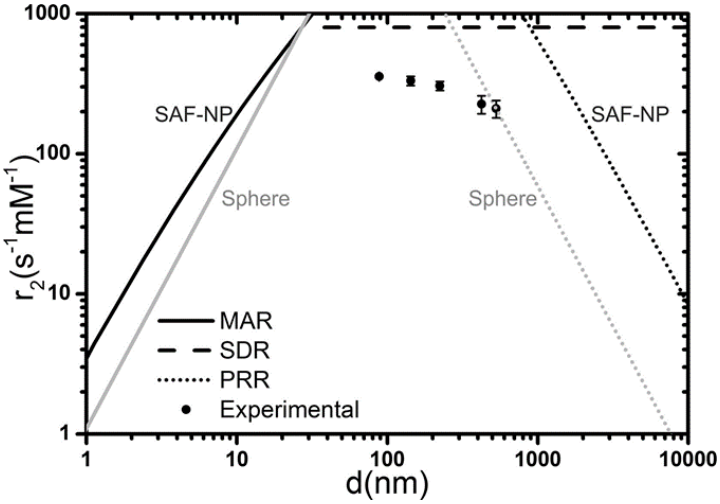

Figure 16: Theoretical (black lines) and measured (points) r_2 values of [Au(10 nm)/NiFe(10 nm)/Au(2.5 nm)/NiFe(10 nm)/Au(10 nm)] SAF-NPs as function of SAF-NP diameter. The reference theoretical values for spherical NiFe particles are represented in gray *[58]*.

6. High-aspect ratio nanowires

Nanowires (NWs) have also been addressed by some reports in the context of this biomedical application. For example, Bañobre-López *et al.* **[57]** evaluated the relaxivity properties of poly-acrylic acid (PAA)-coated Ni ferromagnetic NWs characterized by longitudinal magnetic anisotropy, in a colloidally stable water dispersion. This dispersion has been produced through a process of pulsed electrodeposition of Ni/Gold (Au) multilayer nanowires inside a porous alumina at room-temperature, followed by the template removal and chemical etching of the Au layer in a two-step acidic etching. The relaxation times of these nanostructures, which have presented a monodisperse average diameter and length of ~36 nm and ~600 nm, respectively, have been measured using a relaxometer operated at 60 MHz and under 37 °C for two magnetic fields, namely 1.41 T and 3.0 T. In both situations, the obtained results have indicated that these nanostructures were efficient as T_2 contrast agents, as clearly visible in Figure 17. The contrast effect of the PAA-coated Ni nanowires has been verified by performing an MR scan of a phantom at a magnetic field of 3 T.

Shore et al. **[36]** also studied nanowires for MRI application. Specifically, Fe and segmented Fe/Au nanowires, with various lengths and diameters, have been fabricated by template-assisted electrodeposition. These nanostructures have been coated with compounds, namely Dop-PEG and/or SH-PEG-COOH, which allowed the binding of biological molecules to the nanowires in order to target specific cells. The magnetic characterization of both nanostructures has shown that the Fe/Au nanowires exhibited a larger saturation magnetization. Since Fe layers are thinner than the diameter, these nanostructures were easily magnetized in the direction perpendicular to the long axis of the nanostructure, than in the Fe nanowires. The relaxivity properties of the fabricated nanowires have been measured at 25 °C in a 1.5 T magnetic field and the obtained results have been compared against those of Fe and Fe-Au nanoparticles. As a result, it has beenverified that the Fe nanowires with a length of 0.7 μm and a diameter of 110 nm, coated with Dop-PEG, were the best suited as T_1 contrast agents. On the other hand, Fe-Au nanowires with a length of 1 μm and a diameter of 32.8 nm, coated with SH-PEG-COOH and Dop-PEG, were the most appropriate as T_2 contrast agents, being comparable to commercial Fe oxide nanoparticles. The authors also performed an MR scan of some samples containing Fe and Fe-Au nanowires, at a magnetic field of 9.4 T, in order to confirm the contrast caused by the nanostructures in the image.

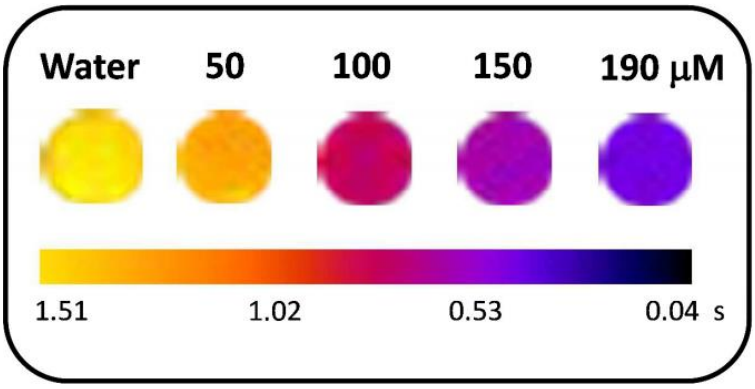

Figure 17: T_2 map associated with PAA-coated Ni nanowires, acquired at 3 T and under 37 ºC *[57]*.

A different type of nanowires for this biomedical application has been investigated by Leung *et al.* [104] .These nanostructures, made from Mn-Fe, have been synthesized through ligand-induced self-organization of Mn–Fe oxide nanoparticles. Then, via TEM, it has been observed that they possessed a mean diameter equal to 35 nm and, on average were 1 µm long. Furthermore, the nanowires elemental content has been verified by inductively coupled plasma-optical emission spectroscopy (ICP-OES), as well as through energy-dispersive X-ray (EDX) spectroscopy, having been determined a Fe percentage of ~40.65. Moreover, their influence in the T_2 relaxation time has been assessed using a 1.5 T MRI system. As a result, it has been noticed that these nanoarchitectures have considerably decreased the MRI signal, when concentrations of 100 µg/mL or 10 µg/mL have been considered, which demonstrated their potential as T_2 contrast agents. Moreover, the cell labelling efficiency of these nanostructures was assessed by incubating them with a macrophage cell line (RAW264.7). After this process, it has been observed an effective Mn-Fe nanowires incorporation into the considered biological entities.

Also considering the improvement of the negative contrast in MRI, Martínez-Banderas *et al.* [105] have fabricated distinct one-dimensional nanostructures, which were composed by an iron core together with an iron oxide shell (Fe-Fe_xO_y core–shell NWs). Then, their r_1, r_2, and r_2/r_1 ratio have been assessed under a 1.5 T magnetic field, having been observed that they possessed a great potential for this application. Furthermore, the effects of various oxidation levels as well as surface coatings have been evaluated at a 7.0 T field. As a result, it has been verified that their r2 could be adjusted by not only the oxide shell thickness, but also coating agents. Moreover, breast cancer cells (MDA-MB-231) labelled with Fe-Fe_xO_y core–shell NWs, which were coated with two different compounds, namely bovine serum albumin (BSA) and (3-aminopropyl)triethoxysilane (APTES), were inserted in tissue-mimicking phantoms. Then, T_2-weighted MR images of those two cases has been performed, having been noticed that the BSA coating improved the dispersion, as well as the cellular internalization, while allowing an identical cell identification efficiency through MRI, when compared against APTES. Consequently, this has permitted the use of a lower nanostructures concentration to efficiently label the desired cells, lowering, therefore, the probability of toxic effects. Furthermore, using such coating, the authors have been able to detect ~25 cells/µL by employing a NW concentration equal to 0.8 µg of Fe/mL. Moreover, cells labelled with BSA coated nanostructures were implanted inside a mouse's

brain and, subsequently, several T2-weighted MR images were acquired, at a 11.7 T field, considering various time intervals post-implantation. As a result, it has been observed that these biological entities could be identified in such organ during, at least, 40 days after insertion.

Iron oxide (Fe_3O_4) nanostructures with rod like morphology (nanowires with low aspect ratio), presenting a diameter of 4–12 nm and length ranging from 30 to 70 nm, were also addressed in the context of this biomedical application by Mohapatra *et al*. [106]. As a result, it was verified that nanorods of 70 nm length showed a r_2 relaxivity of 608 mM^{-1} s^{-1}. Additionally, the increase of the nanorods size led to a linear increase in their r_2 relaxivity values, from 312 to 608 $s^{-1}mM^{-1}$. This linear trend was attributed to an enhancement of the saturation magnetization and the surface area of the nanostructures. Moreover, *in vitro* assays considering HeLa cells indicated that those biological entities exhibited a normal growth in the presence of Fe_3O_4 nanorods, indicating an acceptable biocompatibility without toxic effects (approximately 90 % the cells remained viable), even after incubation with 1 mg/ml of nanorods.

7. Theragnosis Applications

Nanotechnology is a powerful approach for the development of novel nanomaterials that can be used in both the diagnosis and treatment of illnesses, filling, for example, the biggest challenges in the cancer therapeutics. Several types of nanostructures have attracted much attention due to their promising applications as "theragnostic" anti-cancer agents, showing good performance in imaging combined therapy, namely by using hyperthermia, radiotherapy, or drug delivery [102, 107]..

A study by Wang *et al.* [108] reported the construction of an intelligent near-infrared (NIR) light and a tumor microenviroment (NIR/TME) dual-responsive nanocapsule for enhanced tumor accumulation and improved therapy efficacy. The large initial size of these nanocapsules (NCs) ensured the circulatory stability in the blood while, under irradiation of an NIR laser, the shrinkage and decomposition of the nanocapsule in the acidic TME guaranteed intratumoral permeability of NPs and the controllable release of doxorubicin (DOX). Interestingly, the overproduced reactive oxygen species (ROS), by synergistic catalysis of the Fenton reaction based on Fe/FeO NCs and light activation from indocyanine green (ICG), relieved the hypoxia for solid tumors, which is necessary for mitigating the hypoxia-related resistance during chemo/photo- and chemodynamic therapy. As a result of these unique properties of the nanocapsules, it was achieved an almost complete destruction of the tumors. In addition, dual-mode MRI and fluorescence imaging provided complementary imaging information. Hence, this study presented the design of smart nanocapsules with enhanced tumor accumulation, highly effective therapy and diagnosis capability.

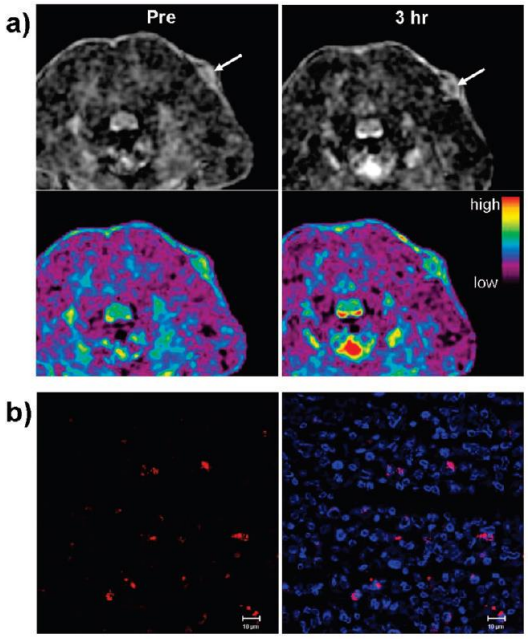

Figure 18: *In vivo* accumulation of Fe_3O_4-MSN at tumor site. (a) *In vivo* T_2-weighted MR images (upper) and color mapped (lower) images of tumor site before and 3 h after intravenous injection of Fe_3O_4-MSN (arrows indicate tumor site). (b) Confocal laser scanning microscopic images of sectioned tumor tissue harvested 24 h after injection. Left: Red fluorescence showing Fe_3O_4-MSN internalized cells. Right: Merged image with 4',6'-diamino-2-fenil-indol (DAPI) stained nuclei (blue) (scale bar) 10 μm). From [109]

Until now, magnetite nanostructures with designed composition and properties are the ones that showed greater potential as theragnostic agents, due to their versatility, biocompatibility, facile production and good magnetic performance for remote *in vitro* and *in vivo* biomedical applications, as presented, for instance, in Figure 18 [109]. This core-shell strategy has given rise to different configurations like single- and multi-core@shell NPs, where magnetite is located in the core (Fe_3O_4@SiO_2; Fe_3O_4@C), in the shell (gelatin-NPs@Fe_3O_4-NPs) or embedded in a polymer matrix (polyester, gelatin magnetic beads). In all cases, the nanocomposites inherit a combination of properties that ensure their multimodal capacities for simultaneous magnetic separation/detection/targeting procedures, like contrast agents in magnetic resonance imaging/positron emission tomography (MRI/PET), magnetic hyperthermia (MH)/drug delivery therapeutic agents, among others [110].

Also, a study by Efremova *et al.* [111] reported the growing of 25 nm octahedral-shaped Fe_3O_4 magnetite nanocrystals on 9 nm Au seed NPs using a modified wet-chemical synthesis. These Fe_3O_4-Au Janus nanoparticles exhibited bulk-like magnetic properties. Additionally, due to their high magnetization and octahedral shape, the hybrids have shown superior *in vitro* and *in vivo* T_2 relaxivity for magnetic resonance imaging as compared to other types of Fe_3O_4-Au hybrids and commercial contrast agents. These nanoparticles provided two functional surfaces for theragnostic applications. Furthermore, for the first time, Fe_3O_4-Au hybrids were conjugated with two fluorescent dyes or a combination of drug and dye, allowing the simultaneous tracking of the nanoparticle vehicle and the drug cargo *in vitro* and *in vivo*. Here, the drug delivery to tumors and payload release has been demonstrated in real time by intravital microscopy. Moreover, replacing the dyes with cell-specific molecules and drugs made the Fe_3O_4-Au hybrids a unique all-in-one platform for theragnostics. Gold and SPION-loaded micelles were also used for both imaging and treatment of brain tumors, serving a theragnostic purpose as both an MRI-based contrast agent and a radiosensitizer [107]. Other

magnetic-gold nanoarchitectures also can be found in the literature as alternatives for theragnosis applications [112, 113].

10. Prospects and Conclusions

The progress in contrast agents for MRI is notorious. Beyond the several contrast agents approved for use in the humans, there are a significant number of new agents in clinical and research development. For this purpose, there is a broad variety of fabrication procedures to obtain paramagnetic and superparamagnetic nanoparticles with a control over their composition, size, and shape. Furthermore, the ability to integrate additional imaging modes or drugs for treatment and the employment of specific vectors linked to the particle surface make these contrast agents yet more promising. More recently, other exciting spin configurations appeared in the literature as potential MRI contrast agents, namely synthetic antiferromagnets (SAFs) and high aspect ratio nanowires (NWs). Biocompatible SAFs nanostructures have been reported with coupling between ferromagnetic layers and their relaxivities and saturation magnetization make them promising for this biomedical application. Also, the characteristics of magnetic NWs and segmented NWs have been explored. As a result, it was observed that the high surface area of these nanostructures and the high magnetic moment also shows an interesting potential for contrast enhancement. The development and comprehension of different magnetic effects has an uttermost importance in the pursuit of novel contrast agents in MRI. On the other hand, systematic *in vivo* studies are also needed so as to understand their mechanism of action and accumulation in the different organs.

Author Contributions: R. Magalhães and S. Caspani revised the major part of the literature and written the several sections with equivalent contributions. J.P. Araújo revised the manuscript. C.T. Sousa structured the review, contributed to write some sections and revised the manuscript.

Acknowledgments: The authors acknowledge funding from the European Union's Horizon 2020 research and innovation program under the Marie Sklodowska-Curie Grant Agreement No. 734801. C.T. Sousa thanks FCT for financial support through the Investigador FCT program (Contract No. IF/01159/2015). R. Magalhães is grateful to the FCT SFRH/BD/148563/2019 PhD grant. This work was also supported by the Portuguese Fundação para a Ciência e Tecnologia (FCT) and COMPETE 2020 (FEDER) under the projects POCI-01-0145-FEDER-028676/PTDC/CTM-CTM/28676/2017,POCI-01-0145/FEDER-032257/PTDC/FIS-OTI/32257/2017, POCI-01-0145-FEDER-031302/PTDC/FIS-MAC/31302/2017, and POCI-01-0141-FEDER-032527.

Conflicts of Interest: The authors declare no conflict of interest.

References

[1] Vadim Kuperman, "Magnetic resonance imaging-physical principles and applications".

[2] H. Shokrollahi, "Contrast agents for MRI," *Materials Science and Engineering* , vol. C 33, pp. 4485-4497, 2013.

[3] Jessica Wahsner, Eric M. Gale, Aurora Rodríguez-Rodríguez, and Peter Caravan, "Chemistry of MRI Contrast Agents: Current Challenges and New Frontiers," *Chemical Reviews,* vol. 119, pp. 957-1057, 2019.

[4] Peter Marckmann, Lone Skov, Kristian Rossen, Anders Dupont, Mette Brimnes Damholt, James Goya Heaf and Henrik S. Thomsen, "Nephrogenic Systemic Fibrosis: Suspected Causative Role of Gadodiamide Used for Contrast-Enhanced Magnetic Resonance Imaging," *Journal of the American Society of Nephrology,* vol. 17, pp. 2359-2362, 2006.

[5] Y. Bao, J. A Sherwood, and Z. Suna, "Magnetic Iron Oxide Nanoparticles as T1 Contrast Agents for Magnetic Resonance Imaging," *Journal of Materials Chemistry C,* 2018.

[6] Quoc Lam Vuong, Pierre Gillis, Yves Gossuin, "Monte Carlo simulation and theory of proton NMR transverse relaxation induced by aggregation of magnetic particles used as MRI contrast agents," *Journal of Magnetic Resonance,* vol. 212, pp. 139-148, 2011.

[7] L. Peixoto, R. Magalhães, D. Navas, S. Moraes, C. Redondo, R. Morales, J. P. Araújo, and C. T. Sousa, "Magnetic nanostructures for emerging biomedical applications," *Applied Physics Reviews,* vol. 7, p. 011310, 2020.

[8] Yu Gao, Yi Liu and Chenjie Xu, "Magnetic Nanoparticles for Biomedical Applications: From Diagnosis to Treatment to Regeneration," em *Engineering in Translational Medicine*.

[9] Yohan Jeong, Hee Sook Hwang & Kun Na, "Theranostics and contrast agents for magnetic resonance imaging," *Biomaterials Research,* vol. 22, 2018.

[10] Yu-Dong Xiao, Ramchandra Paudel, Jun Liu, Cong Ma, Zi-Shu Zhang and Shun-ke Zhou, "MRI contrast agents: Classification and application (Review)," *International Journal of Molecular Medicine,* vol. 38, pp. 1319-1326, 2016.

[11] Tromsdorf UI, Bigall NC, Kaul MG, Bruns OT, Nikolic MS, Mollwitz B, Sperling RA, Reimer R, Hohenberg H, Parak WJ, Förster S, Beisiegel U, Adam G, Weller H., "Size and surface effects on the MRI relaxivity of manganese ferrite nanoparticle contrast agents," *Nano Letters,* vol. 7, pp. 2422-2427, 2007.

[12] Robert-Jan M. van Geuns, Piotr A. Wielopolski, Hein G. de Bruin, Benno J. Rensing, Peter M. A. van Ooijen, Marc Hulshoff, Matthijs Oudkerk, and Pim J. de Feyter, "Basic Principles of Magnetic Resonance Imaging," *Progress in Cariovascular Diseases,* vol. 42, pp. 149-156, 1999.

[13] Hee-Kyung Kim, Gang Ho Lee & Yongmin Chang, "Gadolinium as an MRI contrast agent," *Future Medicinal Chemistry,* 2018.

[14] Juan Pellico, Connor M. Ellis, and Jason J. Davis, "Nanoparticle-Based Paramagnetic Contrast Agents for Magnetic Resonance Imaging," *Hindawi,* 2019.

[15] J. Ramalho, R. C. Semelka, M. Ramalho, R. H. Nunes, M. AlObaidy, and M. Castillo, "Gadolinium-Base Contrast Agent Accumulation and Toxicity: An Update," *American J. of Neuroradiology,* vol. 37, pp. 1192-1198, 2016.

[16] F. Hu and Y. S. Zhao, "Inorganic nanoparticle-based T1 and T1/T2 magnetic resonance contrast probes," *Nanoscale,* vol. 4, p. 6235–6243, 2012.

[17] J. Y. Park, M. J. Baek,E. S. Choi, S. Woo, J. H. Kim, T. J. Kim, J. C. Jung, K. S. Chae, Y. Chang, G. H. Lee, "Paramagnetic ultrasmall gadolinium oxide nanoparticles as advanced T1 MRI contrast agent: account for large longitudinal relaxivity, optimal particle diameter, and in vivo T1 MR images," *ACS nano,* vol. 3, p. 3663–3669, 2009.

[18] Hyon Bin Na, Jung Hee Lee, Kwangjin An, Yong Il Park, Mihyun Park, In Su Lee, Do-Hyun Nam, Sung Tae Kim, Seung-Hoon Kim, Sang-Wook Kim, Keun-Ho Lim, Ki-Soo Kim, Sun-Ok Kim, Taeghwan Hyeon, "Development of a T1 Contrast Agent for Magnetic Resonance Imaging Using MnO Nanoparticles," *Angewandte Chemie International Edition,* vol. 46, 2007.

[19] Kashmiri Deka, Anupam Guleria, Dinesh Kumar, Jayeeta Biswas, Saurabh Lodha, Som Datta Kaushik, Suman Dasgupta, Pritam Deb, "Mesoporous 3D carbon framework encapsulated manganese oxide nanoparticles as biocompatible T1 MR imaging probe," *Colloids and Surfaces A: Physicochemical and Engineering Aspects,* vol. 539, pp. 229-236, 2018.

[20] Gurvinder Singh, Birgitte Hjelmeland McDonagh,Sjoerd Hak, Davide Peddis, Sulalit Bandopadhyay, Ioanna Sandvig, Axel Sandvigef and Wilhelm R. Glommbg, "Synthesis of gadolinium oxide nanodisks and gadolinium doped iron oxide nanoparticles for MR contrast agents," *Journal of Materials Chemistry B,* vol. 5, pp. 418-422, 2017.

[21] X.-Y. Zheng, J. Pellico, A. A. Khrapitchev, N. R. Sibson, and J. J. Davis, "Dy-DOTA integrated mesoporous silica nanoparticles as promising ultrahigh field magnetic resonance imaging contrast agents," *Nanoscale,* vol. 10, p. 21041–21045, 2018.

[22] I. Craciun, G. Gunkel-Grabole, A. Belluati, C. G. Palivan, and W. Meier, "Expanding the potential of MRI contrast agents through multifunctional polymeric nanocarriers," *Nanomedicine,* vol. 12, pp. 811-817, 2017.

[23] Yuqi Yang, Shizhen Chen, Haidong Li, Yaping Zhang, Junshuai Xie, Dennis W. Hwang, Aidong Zhang, Maili Liu and Xin Zhou, "Engineered Paramagnetic Graphene Quantum Dots with Enhanced Relaxivity for Tumor Imaging," *Nano Letters,* vol. 19, pp. 441-448, 2018.

[24] Lucio Litti, Niccolò Rivato, Giulio Fracasso, Pietro Bontempi, Elena Nicolato, Pasquina Marzola, Alfonso Venzo, Marco Colombatti, Marina Gobbo and Moreno Meneghetti, "A SERRS/MRI multimodal contrast agent based on naked Au nanoparticles functionalized with a Gd(iii) loaded PEG polymer for tumor imaging and localized hyperthermia," *Nanoscale,* vol. 10, p. 1272–1278, 2018.

[25] T. Vangijzegem, D. Stanicki, S. Boutry, Q. Paternoster, L. Vander Elst, R.N. Muller, S. Laurent1, "VSION as high field MRI T1 contrast agent: evidence of their potential as positive contrast agent for magnetic resonance angiography," *Nanotechnology,* 2018.

[26] Elena Taboada, Elisenda Rodríguez, Anna Roig, Judit Oró, Alain Roch and Robert N. Muller, "Relaxometric and Magnetic Characterization of Ultrasmall Iron Oxide Nanoparticles with High Magnetization. Evaluation as Potential T1 Magnetic Resonance Imaging Contrast Agents for Molecular Imaging," *Langmuir,* vol. 23, pp. 4583-4588, 2007.

[27] U. I. Tromsdorf, O. T. Bruns, S. C. Salmen, U. Beisiegel, H. Weller, "A highly effective, nontoxic T1 MR contrast agent based on ultrasmall PEGylated iron oxide nanoparticles," *Nano Letters,* vol. 9, pp. 4434-40, 2009.

[28] B. H. Kim, N. Lee, H. Kim, K. An, Y. I. Park, Y. Choi, K. Shin, Y. Lee, S. G. Kwon, H. B. Na, J. G. Park, T. Y. Ahn, Y. W. Kim, W. K. Moon, S. H. Choi, T. Hyeon, "Large-scale synthesis of uniform and extremely small-sized iron oxide nanoparticles for high-resolution T1 magnetic

resonance imaging contrast agents," *Journal of the American Chemical Society,* vol. 133, pp. 12624-31, 2011.

[29] Fengqin Hu, Qiaojuan Jia, Yilin Li and Mingyuan Gao, "Facile synthesis of ultrasmall PEGylated iron oxide nanoparticles for dual-contrast T1- and T2-weighted magnetic resonance imaging".

[30] Fengqin Hu, Keith W. MacRenaris, Emily A. Waters, Taiyang Liang, Elise A. Schultz-Sikma, Amanda L. Eckermann, and Thomas J. Meade, "Ultrasmall, Water-Soluble Magnetite Nanoparticles with High Relaxivity for Magnetic Resonance Imaging," *The Journal of Physical Chemistry,* vol. 113, p. 20855–20860, 2009.

[31] Bo Chen, Zhanhang Guo, Chunxian Guo,a Yu Mao, Zhiguo Qin, Dewen Ye, Fengchao Zang, Zhichao Lou, Zuoheng Zhang, Mingyue Li, Yanlong Liu,f Min Ji, Jianfei Sunb and Ning Gu, "Moderate cooling coprecipitation for extremely small iron oxide as a pH dependent T1-MRI contrast agent," *Nanoscale,* 2020.

[32] Zheyu Shen, Tianxiang Chen, Xuehua Ma, Wenzhi Ren, Zijian Zhou, Guizhi Zhu, Ariel Zhang, Yijing Liu, Jibin Song, Zihou Li, Huimin Ruan, Wenpei Fan, Lisen Lin, JeevaMunasinghe, Xiaoyuan Chen, Aiguo Wu, "Multifunctional Theranostic Nanoparticles Based on Exceedingly Small Magnetic Iron Oxide Nanoparticles for T1-Weighted Magnetic Resonance Imaging and Chemotherapy," *ACS nano,* 2017.

[33] Thomas Macher, John Totenhagen, Jennifer Sherwood, Ying Qin, Demet Gurler, Mark S. Bolding, Yuping Bao, "Ultrathin Iron Oxide Nanowhiskers as Positive Contrast Agents for Magnetic Resonance Imaging," *Advanced Functional Materials,* vol. 25, 2014.

[34] Yuping Bao, Tianlong Wen, Anna Cristina S. Samia, Amit Khandhar and Kannan M. Krishnan, "Magnetic Nanoparticles: Material Engineering and Emerging Applications in Lithography and Biomedicine," *Journal of Materials Science,* vol. 51, p. 513–553, 2017.

[35] Ken Cham-Fai Leung and Yi-Xiang J. Wang, "Mn–Fe Nanowires Towards Cell Labeling and Magnetic Resonance Imaging," *Nanowires Science and Technology,* 2010.

[36] Daniel Shore, Sylvie L. Pailloux, Jinjin Zhang, Thomas Gage, David J. Flannigan, Michael Garwood, Valérie C. Pierre and Bethanie J. H. Stadler, "Electrodeposited Fe and Fe–Au

nanowires as MRI contrast agents," *Chemical Communications,* vol. 52, pp. 12634-12637, 2016.

[37] Jennifer Sherwood, "SHAPE DEPENDENT IRON OXIDE NANOPARTICLES FOR SIMULTANEOUS IMAGING AND THERAPY," 2018.

[38] Zhen Li, Pei Wei Yi, Qiao Sun, Hao Lei, Hong Li Zhao, Zhong Hua Zhu, Sean C. Smith, Min Bo Lan, and Gao Qing (Max) Lu, "Ultrasmall Water-Soluble and Biocompatible Magnetic Iron Oxide Nanoparticles as Positive and Negative Dual Contrast Agents," *Advanced Functional Materials,* vol. 22, p. 2387–2393, 2012.

[39] V. K. Sharma, A. Alipour, Z. Soran-Erdem, Z. G. Aykuta and H. V. Demir, "Highly monodisperse low-magnetization magnetite nanocubes as simultaneous T1–T2 MRI contrast agents," *Nanoscale,* vol. 7, p. 10519–10526, 2015.

[40] Guoming Huang, Hui Li, Jiahe Chen, Zhenghuan Zhao, Lijiao Yang, Xiaoqin Chi, Zhong Chen, Xiaomin Wangb and Jinhao Gao, "Tunable T1 and T2 contrast abilities of manganese-engineered iron oxide nanoparticles through size control," *Nanoscale,* vol. 6, p. 10404, 2014.

[41] Mark J. Bailey, Rob van der Weegen, Piper J. Klemm, Suzanne L. Baker, and Brett A. Helms, "Stealth Rare Earth Oxide Nanodiscs for Magnetic Resonance Imaging," *Advanced Healthcare Materials,* vol. 1, pp. 437-442, 2012.

[42] Serena A. Corr, Stephen J. Byrne, Renata Tekoriute, Carla J. Meledandri, Dermot F. Brougham Marina Lynch, Christian Kerskens, Laurence O'Dwyer, and Yurii K. Gun'ko, "Linear Assemblies of Magnetic Nanoparticles as MRI Contrast Agents," *Journal of American Chemical Society,* vol. 130, pp. 4214-4215, 2008.

[43] Yung-Kang Peng, Chien-Liang Liu, Hsieh-Chih Chen, Shang-Wei Chou, Wei-Hsuan Tseng Yu-Jui Tseng, Chia-Cheng Kang, Jong-Kai Hsiao, and Pi-Tai Chou, "Antiferromagnetic Iron Nanocolloids: A New Generation in Vivo T1 MRI Contrast Agent," *Journal of the American Chemical Society,* pp. 18621-18628, 2013.

[44] Herbert R. Neves, Rafael A. Bini, Jeam H. O. Barbosa, Carlos E. G. Salmon ,and Laudemir C. Varanda, "Dextran-Coated Antiferromagnetic MnO Nanoparticles for a T 1 -MRI Contrast

Agent with High Colloidal Stability," *Particle & Particle Systems Characterization,* vol. 33, p. 167–176, 2016.

[45] Wells Mangrum, Quoc Bao Hoang, Tim J. Amrhein, Scott M. Duncan, Charles M. Maxfield, Elmar Merkle, Allen W. Song, Duke Review of MRI Principles:Case Review Series E-Book, Elsevier Health Sciences, 2018.

[46] M. A. Fogel, Principles and Practice of Cardiac Magnetic Resonance in Congenital Heart Disease: Form, Function and Flow, Wiley, 2010.

[47] Tina Lam, Philippe Pouliot, Pramod K. Avti, Frédéric Lesage, Ashok K. Kakkar, "Superparamagnetic iron oxide based nanoprobes for imaging and theranostics," *Advances in Colloid and Interface Science,* Vols. %1 de %2199-200, pp. 95-113, 2013.

[48] Nohyun Lee and Taeghwan Hyeon, "Magnetic Nanoparticles for Magnetic Resonance Imaging Contrast Agents," em *Magnetic Nanoparticles in Biosensing and Medicine*, 2019, pp. 228-250.

[49] Joan Estelrich, María Jesús Sánchez-Martín, Maria Antònia Busquets, "Nanoparticles in magnetic resonance imaging: from simple to dual contrast agents," *International Journal of Nanomedicine,* vol. 10, pp. 1727-1741, 2015.

[50] Tae-Hyun Shin, Jin-sil Choi, Seokhwan Yun, Il-Sun Kim, Ho-Taek Song, Youngmee KimKook In Park, and Jinwoo Cheon, "T1 and T2 Dual-Mode MRI Contrast Agent for Enhancing Accuracy by Engineered Nanomaterials," *ACS nano,* vol. 8, p. 3393–3401, 2014.

[51] Zapotoczny, Agnieszka Szpak • Sylwia Fiejdasz • Witold PrendotaTomasz Stra˛czek • Czesław Kapusta • Janusz SzmydMaria Nowakowska • Szczepan, "T1–T2 Dual-modal MRI contrast agents based on superparamagnetic iron oxide nanoparticles with surface attached gadolinium complexes," *Journal of Nanoparticle Research,* vol. 16, p. 2678, 2014.

[52] Li Li, Wen Jiang, Kui Luo, Hongmei Song, Fang Lan, Yao Wu and Zhongwei Gu, "Superparamagnetic Iron Oxide Nanoparticles as MRI contrast agents for Non-invasive Stem Cell Labeling and Tracking," *Theranostics,* vol. 3, pp. 595-615, 2013.

[53] S. Boutry, R.N. Muller, S. Laurent, "Targeted Iron Oxide (Nano)particles Used as MRI Contrast Agent in Small Animal Models," em *Iron Oxide Nanoparticles for Biomedical Applications*, 2018, pp. 135-158.

[54] Catherine C. Berry and Adam S. G. Curtis, "Functionalisation of magnetic nanoparticles for applications in biomedicine," *Journal of Physics D: Applied Physics,* vol. 36, pp. R198-R206, 2003.

[55] J. S. Michael, B. S. Lee, M. Zhang, J.S. Yu, "Nanotechnology for Treatment of Glioblastoma Multiforme," *Journal of Translational Internal Medicine,* vol. 6, pp. 128-133, 2018.

[56] An-Hui Lu, E. L. Salabas, and Ferdi Schuth, "Magnetic Nanoparticles: Synthesis, Protection, Funcionalization, and Application," *Angewandte Chemie,* vol. 46, pp. 1222-1244, 2007.

[57] Manuel Banobre-Lopez, Cristina Bran, Carlos Rodriguez-Abreu, Juan Gallo, Manuel Vazquez and Jose Rivas, "A colloidally stable water dispersion of Ni nanowires as an efficient T2-MRI contrast agent," *Journal of Material Chemistry B,* vol. 5, pp. 3338-3347, 2017.

[58] Ruben Van Roosbroeck, Willem Van Roy, Tim Stakenborg, Jesse Trekker, Antoine D'Hollander, Tom Dresselaers, Uwe Himmelreich, Jeroen Lammertyn, and Liesbet Lagae, "Synthetic Antiferromagnetic Nanoparticles as Potential Contrast Agents in MRI," *American Chemical Society,* vol. 8, pp. 2269-2278, 2014.

[59] Arati G. Kolhatkar 1, Andrew C. Jamison 1, Dmitri Litvinov 1,2,3,*, Richard C. Willson 2,*and T. Randall Lee 1,*, "Tuning the Magnetic Properties of Nanoparticles," *International Journal of Molecular Science,* vol. 14, pp. 15977-16009, 2013.

[60] Abolfazl Akbarzadeh, Mohamad Samiei and Soodabeh Davaran, "Magnetic nanoparticles: preparation, physical properties, and applications in biomedicine," *Nanoscale Research Letters,* vol. 7, p. 144, 2012.

[61] Kai Wu, Diqing Su, Jinming Liu, Renata Saha, and Jian-Ping Wang, "Magnetic Nanoparticles in Nanomedicine," 2018.

[62] Q. A. Pankhurst, J. Connolly, S. K. Jones and J. Dobson, "Application of magnetic nanoparticles in biomedicine," *J. of Physics D: Applied Physics,* vol. 36, pp. R167-R181, 2003.

[63] Chenjie Xu and Shouheng Sun, "Monodisperse magnetic nanoparticles for biomedical applications," *Polymer International,* vol. 56, pp. 821-826, 2007.

[64] Vanessa Fernandes Cardoso, António Francesko, Clarisse Ribeiro, Manuel Bañobre-López,Pedro Martins,* and Senentxu Lanceros-Mendez, "Advances in Magnetic Nanoparticles for Biomedical Applications," *Adv. Healthcare Mater.,* vol. 7, p. 1700845, 2008.

[65] A.L. Koh, W. Hu, R.J. Wilson, S.X. Wang & R. Sinclair, "Preparation, structural and magnetic characterization of synthetc anti-ferromagnetic nanoparticles," *Philosophical Magazine,* vol. 88, pp. 4225-4241, 2008.

[66] P. Bruno, "Theory of interlayer exchange interactions in magnetic multilayers," *J. of Physics: Condensed Matter,* vol. 11, p. 9403, 1999.

[67] P. Bruno and C. Chappert, "Oscillatory Coupling between Ferromagnetic Layers Separated by a Nonmagnetic Metal Spacer," *Physical Review Letters,* vol. 67, p. 2592, 1991.

[68] B. Dieny, J. P. Gavigan, and J. P. Rebouillat, "Magnetisation processes, hysteresis and finite-size effects in model multilayer systems of cubic or uniaxial anisotropy with antiferromagnetic coupling between adjacent ferromagnetic layers," *J. of Physics: Condensed Matter,* vol. 2, pp. 159-185, 1990.

[69] Wei Hu, Robert J. Wilson, Christopher M. Earhart, Ai Leen Koh, Robert Sinclair, and Shan X. Wang, "Synthetic antiferromagnetic nanoparticles with tunable susceptibilities," *Applied Physics ,* vol. 105, p. 07B508, 2009.

[70] M. Susano, M. P. Proenca, S. Moraes, C. T. Sousa and J. P. Araújo, "Tuning the magnetic properties of multisegmented Ni/Cu electrodeposited nanowires with controllable Ni lengths," *Nanotechnology,* vol. 27, p. 335301, 2016.

[71] Anthony S. Arrott, Bretislav Heinrich, and Amikan Aharoni, "Point Singularities and Magnetization Reversal in Ideally soft Ferromagnetic Cylinders," *IEEE Transaction on Magnetics,* vol. 15, p. 1228, 1979.

[72] E. H. Frei, S. Shtrikman, and D. Treves, "Critical Size and Nucleation Field of Ideal Ferromagnetic Particles," *Physical Review,* vol. 106, p. 446, 1957.

[73] E. C. Stoner, F. R. S and E. P. Wohlfarth, A mechanism of magnetic hysteresis in heterogeneous alloys.

[74] Raluca M. Fratila, Sara Rivera-Fernandez and Jeus M. de la Fuente, "Shape matters: synthesis and biomedical applications of high aspect ratio magnetic nanomaterials," *Nanoscale,* vol. 7, p. 8233, 2015.

[75] Bashar Issa and Ihab M. Obaidat, "Magnetic Nanoparticles as MRI Contrast Agents," em *Magnetic Resonance Imaging*, 2019.

[76] Yasir Javed, Kanwal Akhtar, Hafeez Anwar, Yasir Jamil, "MRI based on iron oxide nanoparticles contrast agents: effect of oxidation state and architecture," *Journal of Nanoparticle Research,* vol. 19, p. 366, 2017.

[77] Ibrahim Khan, Khalid Saeed, and Idrees Khan, "Nanoparticles: Properties, applications and toxicities," *Arabian Journal of Chemistry,* vol. 12, pp. 908-931, 2019.

[78] Karrina McNamara and Syed A. M. Tofail, "Nanoparticles in biomedical applications," *Advances in Physics: X,* vol. 2, pp. 54-88, 2017.

[79] Association, I. R. Managment, Pharmaceutical Sciences: Breakthroughs in Research and Practice, 2016.

[80] Nicholas J Hobson, Xian Weng, Bernard Siow, Catarina Veiga, Marianne Ashford, Nguyen TK Thanh, Andreas G, Schätzlein & Ijeoma F. Uchegbu, "Clustering superparamagnetic iron oxide nanoparticles produces organ-targeted high-contrast magnetic resonance images," *Nanomedicine,* vol. 14, pp. 1135-1152, 2019.

[81] Brice Basly, "Dendronized iron oxide nanoparticles as contrast agents for MRI," *Chemical Communications,* vol. 46, pp. 985-987, 2010.

[82] H. Xie, Y. Zhu, W. Jiang, Q. Zhou, H. Yang, N. Gu, Y. Zhang, H. Xu, H. Xu, X. Yang, "Lactoferrin-conjugated superparamagnetic iron oxide nanoparticles as a specific MRI contrast agent for detection of brain glioma in vivo," *Biomaterials,* vol. 32, pp. 495-502, 2011.

[83] Roberto Gonzalez-Rodriguez, Elizabeth Campbell, Anton Naumov, "Multifunctional graphene oxide/iron oxide nanoparticles for magnetic targeted drug delivery dual magnetic resonance/fluorescence imaging and cancer sensing," *PLoS ONE,* vol. 14, 2019.

[84] Selim Sulek, a Busra Mammadov, Davut I. Mahcicek, Huseyin Sozeri, Ergin Atalar, Ayse B. Tekinaya and Mustafa O. Guler, "Peptide functionalized superparamagnetic iron oxide nanoparticles as MRI contrast agents," *Journal of Materials Chemistry,* vol. 21, pp. 15157-15162, 2011.

[85] Lamiaa MA Ali, Pasquina Marzola, Elena Nicolato, Silvia Fiori, Marcelo de las Heras Guillamón, Rafael Piñol, Lierni Gabilondo, Angel Millán, and Fernando Palacio, "Polymer-coated superparamagnetic iron oxide nanoparticles as T2 contrast agent for MRI and their uptake in liver," *Future Science OA,* 2017.

[86] Yancong Zhang, Lianying Zhang, Xinfeng Song, Xiangling Gu, Hanwen Sun ,Chunhua Fu, and Fanzong Meng, "Synthesis of Superparamagnetic Iron Oxide Nanoparticles Modified with MPEG-PEI via Photochemistry as New MRI Contrast Agent," *Journal of nanomaterials,* 2015.

[87] T. J. X. F. Z. J.-B. G. N. Z. Y.-H. D. Y. G. L. Yue-Jian, "Synthesis, self-assembly, and characterization of PEG-coated iron oxide nanoparticles as potential MRI contrast agent," *Drug development and industrial pharmacy,* vol. 36, pp. 20101235-1244, 2010.

[88] Joel Garcia, Stephen Z. Liu, and Angelique Y. Louie, "Biological effects of MRI contrast agents: gadolinium retention, potential mechanisms and a role for phosphorus," *Philosophical Transactions of the Royal Society A: Mathematical, Physical and Engineering Sciences,* vol. 375, p. 20170180, 2017.

[89] Z. Dai, Advances in Nanotheranostics II: Cancer Theranostic Nanomedicine, 2016.

[90] H. Wei, O. T. Bruns, M. G. Kaul, E. C. Hansen, M. Barch, A. Wiśniowska, O. Chen, Y. Chen, N. Li, S. Okada, J. M. Cordero, M. Heine, C. T. Farrar, D. M. Montana, G. Adam, H. Ittrich, A. Jasanoff, P. Nielsen, M. G. Bawendi, "Exceedingly small iron oxide nanoparticles as positive MRI contrast agents," *Proceedings of the National Academy of Sciences of the United States of America,* vol. 114, pp. 2325-2330, 2017.

[91] X. Yin, S. E. Russek, G. Zabow, F. Sun, J. Mohapatra, K. E. Keenan, M. A. Boss, H. Zeng, J. P. Liu, A. Viert, S. H. Liou, J. Moreland, "Large T1 contrast enhancement using superparamagnetic nanoparticles in ultra-low field MRI," *Scientific Reports,* vol. 8, p. 11863, 2018.

[92] William J. Rieter, Jason S. Kim, Kathryn M.L. Taylor, Hongyu An, Weili Lin, Teresa Tarrant, Wenbin Lin, "Hybrid silica nanoparticles for multimodal imaging," *Angewandte Chemie - International Edition,* vol. 46, pp. 3680-3682, 2007.

[93] J. J. Davis, W-Y Huang, G-L Davies, "Location-tuned relaxivity in Gd-doped mesoporous silica nanoparticles," *JOURNAL OF MATERIALS CHEMISTRY,* vol. 22, p. 22848–22850, 2012.

[94] W. Y. Huang, G. L. Davies and J. J. Davis, "High signal contrast gating with biomodified Gd doped mesoporous nanoparticles," *Chemical Communications,* vol. 49, pp. 60-62, 2013.

[95] Mengxin Zhang, Xiaoyun Liu, Jie Huang, Lina Wang, He Shen, Yu Luo, Zhenjun Li, Hailu Zhang, Zongwu Deng, Zhijun Zhang, "Ultrasmall graphene oxide based T1 MRI contrast agent for in vitro and in vivo labeling of human mesenchymal stem cells," *Nanomedicine: Nanotechnology, Biology and Medicine,* vol. 14, pp. 2475-2483, 2018.

[96] Alexander M. Panich, Moti Salti, Shaul D. Goren, Elena Yudina, A. E. Aleksenskii, Alexander Ya. Vul, Alexander I. Shames, "Gd(III)-Grafted Detonation Nanodiamonds for MRI Contrast Enhancement," *The Journal of Physical Chemistry C,* vol. 123, p. 2627−2631, 2019.

[97] L. Xu, S. H. Hong, Y. Sun, Z. Sun, K. Shou, K. Cheng, H. Chen, D. Huang, H. Xu, Z. Cheng, "Dual T1 and T2 weighted magnetic resonance imaging based on Gd3+ loaded bioinspired melanin dots.," *Nanomedicine,* vol. 14, pp. 1743-1752, 2018.

[98] Jinchang Yin, Deqi Chen, Yu Zhang, Chaorui Li, Lizhi Liu and Yuanzhi Shao, "MRI relaxivity enhancement of gadolinium oxide nanoshells with a controllable shell thickness," *Physical Chemistry Chemical Physics,* vol. 20, pp. 10038-10047, 2018.

[99] Y. Zeng, L. Wang, Z. Zhou, X. Wang, Y. Zhang, J. Wang, P. Mi, G. Liu, L. Zhou, "Gadolinium hybrid iron oxide nanocomposites for dual T1- and T2-weighted MR imaging of cell labeling.," *Biomaterials science,* vol. 5, pp. 50-56, 2016.

[100] Vincent Jacques, Stephane Dumas, Wei-Chuan SUn, Jeffry S. Troughton, Matthew T. Greenfield and Peter Caravan, "High-Relaxivity Magnetic Resonance Imaging Contrast Agents Part 2," *Investigative Radiology,* vol. 45, pp. 613-624, 2010.

[101] Kashmiri Deka, Anupam Guleria, Dinesh Kumar, Jayeeta Biswas, Saurabh Lodha, Som Datta Kaushik, Suman Dasgupta, Pritam Deb, "Title: Mesoporous 3D Carbon Framework Encapsulated Manganese Oxide Nanoparticles as Biocompatible T1 MR Imaging Probe," *Colloids and Surfaces A: Physicochemical Engineering Aspects,* vol. 539, pp. 229-236, 2018.

[102] Zhenghuan Zhao, Chengjie Sun, Jianfeng Bao, Lijiao Yang, Ruixue Wei, Jingliang Cheng, Hongyu Lina and Jinhao Gao, "Surface manganese substitution in magnetite nanocrystals enhances T1 contrast ability by increasing electron spin relaxation," *Journal of Materials Chemistry B,* vol. 6, pp. 401-413, 2018.

[103] Chien-Liang Liu, Yung-Kang Peng, Shang-Wei Chou, Wei-Hsuan Tseng, Yu-Jui Tseng, Hsieh-Chih Chen, Jong-Kai Hsiao, Pi-Tai Chou, "One-Step, Room-Temperature Synthesis of Glutathione-Capped Iron-Oxide Nanoparticles and their Application in In Vivo T1-Weighted Magnetic Resonance Imaging," *Small,* vol. 10, pp. 3962-3969, 2014.

[104] Ken Cham-Fai Leung, Yi-Xiang J. Wang, Hao-Hao Wang, Chun-Pong Chak, "Novel one-dimensional Mn—Fe oxide nanowires for cell labeling and magnetic resonance imaging," *International Conference on Information Technology and Applications in Biomedicine,* pp. 193-195, 2008.

[105] Aldo Isaac Martínez-Banderas, Antonio Aires, Sandra Plaza-García, Lorena Colás, Julián A. Moreno, Timothy Ravasi, Jasmeen S. Merzaban, Pedro Ramos-Cabrer, Aitziber L.

Cortajarena & Jürgen Kosel, “Magnetic core–shell nanowires as MRI contrast agents for cell tracking,” *Journal of Nanobiotechnology,* vol. 18, pp. 1-12, 2020.

[106] Jeotikanta Mohapatra, Arijit Mitra, Himanshu Tyagi, D. Bahadur and M. Aslam, “Iron oxide nanorods as high-performance magnetic resonance imaging contrast agents,” *Nanoscale,* vol. 7, pp. 9174-9184, 2015.

[107] Sun L., Joh D.Y., Al-Zaki A., Stangl M., Murty S., Davis J.J., Baumann B.C., Alonso-Basanta M., Kaol G.D., Tsourkas A., Dorsey J.F., “Theranostic Application of Mixed Gold and Superparamagnetic Iron Oxide Nanoparticle Micelles in Glioblastoma Multiforme,” *Journal of Biomedical Nanotechnology,* vol. 12, pp. 347-356, 2016.

[108] Zhiyi Wang, Yanmin Ju, Zeeshan Ali, Hui Yin, Fugeng Sheng, Jian Lin, Baodui Wang & Yanglong Hou, “Near-infrared light and tumor microenvironment dual responsive size-switchable nanocapsules for multimodal tumor theranostics,” *Nature Communications,* vol. 10, 2019.

[109] Ji Eun Lee, Nohyun Lee, Hyoungsu Kim, Jaeyun Kim, Seung Hong Choi, Jeong Hyun Kim, Taeho Kim, In Chan Song, Seung Pyo Park, Woo Kyung Moon, and Taeghwan Hyeon, “Uniform Mesoporous Dye-Doped Silica Nanoparticles Decorated with Multiple Magnetite Nanocrystals for Simultaneous Enhanced Magnetic Resonance Imaging, Fluorescence Imaging, and Drug Delivery,” *Journal of American Chemical Society,* vol. 132, p. 552–557, 2010.

[110] Yolanda Piñeiro, Manuel González Gómez, Lisandra de Castro Alves, Angela Arnosa Prieto, Pelayo García Acevedo, Román Seco Gudiña, Julieta Puig, Carmen Teijeiro, Susana Yáñez Vilar and José Rivas, “Hybrid Nanostructured Magnetite Nanoparticles: From Bio-Detection and Theragnostics to Regenerative Medicine,” *magnetochemistry,* vol. 6, 2020.

[111] Maria V. Efremova, Victor A. Naumenko, Marina Spasova, Anastasiia S. Garanina, ,Maxim A. Abakumov, Anastasia D. Blokhina, Pavel A. Melnikov, Alexandra O. Prelovskaya,Markus Heidelmann, Zi-An Li, Zheng Ma, Igor V. Shchetinin2 et. al, “Magnetite-Gold nanohybrids as ideal all-in-one platforms for theranostics”.

[112] C. T. Sousa, D. C. Leitao, J. Ventura, P. B. Tavares, J. P. Araújo, "A versatile synthesis method of dendrites-free segmented nanowires with a precise size control," *Nanoscale Research Letters,* vol. 7, p. 168, 2012.

[113] Ana Espinosa, Jelena Kolosnjaj-Tabi, Ali Abou-Hassan, Anouchka Plan Sangnier, Alberto Curcio, Amanda K. A. Silva, Riccardo Di Corato, Sophie Neveu, Teresa Pellegrino, Luis M. Liz-Marzán, Claire Wilhelm, "Magnetic (Hyper)Thermia or Photothermia? Progressive Comparison of Iron Oxide and Gold Nanoparticles Heating in Water, in Cells, and In Vivo," *Advanced Functional Materials,* vol. 28, p. 1803660, 2018.